NCAR CESM2 release of CAM-SE: A reformulation of the spectral-element dynamical core in dry-mass vertical coordinates with comprehensive treatment of condensates and energy

P. H. Lauritzen[1]*, R.D. Nair[1], A.R. Herrington[2],P. Callaghan[1], S. Goldhaber[1], J.M. Dennis[1], Julio T. Bacmeister[1], B. Eaton[1], C.M. Zarzycki[1], A. Gettelman[1], R.B. Neale[1], B. Dobbins[1], Mark A. Taylor[3], K.A. Reed[2]

[1]National Center for Atmospheric Research
[2]School of Marine and Atmospheric Sciences, Stony Brook University, State University of New York, Stony Brook, New York
[3]Sandia National Laboratories, Albuquerque, New Mexico

Key Points:

- = enter point 1 here =
- = enter point 2 here =
- = enter point 3 here =

*1850 Table Mesa Drive, Boulder, Colodaro, USA

Corresponding author: peter Hjort Lauritzen, pel@ucar.edu

Abstract

It is the purpose of this paper to document and validate the new NCAR version of the spectral-element (SE) dynamical core as part of the CESM2.0 release. This version differs from previous releases of the SE dynamical core in several ways. Most notably the hybrid-sigma vertical coordinate is based on dry pressure, the condensates are dynamically active in the thermodynamic and momentum equations (also referred to as condensate loading), and the continuous equations of motion conserve a more comprehensive total energy that includes condensates. The code base has been significantly reduced and cleaned up as part of integrating SE as a dynamical core in the CAM (Community Atmosphere Model) repository rather than importing the SE dynamical core from HOMME (high-order method modeling environment) as an external code.

1 Introduction

[reference relevant spectral-element dycores: Giraldo, Marras, etc.]

For a while the Community Earth System Model [CESM; *Hurrell et al.*, 2013] has had a highly scalable dynamical core option in the atmosphere component CAM [Community Atmosphere Model; *Neale et al.*, 2010] based on the spectral-element (SE) method discretized on the cubed-sphere. The SE model supports uniform resolution grids based on the equi-angular gnomonic cubed-sphere grid and a mesh-refinement configuration with local increases in resolution through conformal mesh-refinement [*Fournier et al.*, 2004; *Baer et al.*, 2006; *Zarzycki et al.*, 2013, 2014]. The dynamical core code resided in the High-Order Methods Modeling environment (HOMME) which is a framework for developing new generation computationally efficient and petascale capable dynamical cores based on the SE method [*Thomas and Loft*, 2000; *Taylor et al.*, 2008], the discontinuous Galerkin method [*Nair et al.*, 2009] and finite-volume method [*Erath et al.*, 2012; *Lauritzen et al.*, 2017]. The SE dynamical core was imported into CAM as an external code base. Consequently any updates to the HOMME code base would have to be imported into CAM and pass regression tests in both HOMME and CAM. We refer to this setup as CAM-HOMME which has been tested quite extensively for AMIP-style climate simulation [*Evans et al.*, 2012; *Bacmeister et al.*, 2013; *Reed et al.*, 2015].mention cubed-sphere and mesh-refinement

With the department of energy (DOE) branching from the CESM to develop their on Earth System Model using their own code base, NCAR decided to no longer import HOMME as an external code base in CAM due to the cumbersome software engineering involved in maintaining two code bases and having to support configurations in HOMME not used in CAM. Instead the SE configuration of HOMME became part of the CAM code base. With that came a massive code clean-up to satisfy software engineering standards in CAM (and make the code more user-friendly for the community) as well as considerable science changes described in this paper.

The SE dynamical core is the default dynamical core for high-resolution CESM applications, in particular, the configuration in which the average distance between grid-point is approximately 25km [*Bacmeister et al.*, 2013]. At such resolutions the effects of condensates (such as cloud liquid and ice) may have a significant effect on the dynamics [*Bacmeister et al.*, 2012]. CAM-HOMME does not represent the effect of condensates in the thermodynamic and momentum equations (also referred to as condensate loading). Representing condensates in the dynamical core is easier when using a dry-mass hybrid-sigma vertical coordinate than when using the usual moist-mass hybrid-sigma vertical coordinate [e.g., *Simmons and Burridge*, 1981]. In other words, the model levels are defined in terms of dry atmosphere surface pressure rather than moist (full) surface pressure.

A second motivation for switching to a dry-mass vertical coordinate is the physical parameterizations. CAM physics assumes that the moist pressure levels are constant during the parameterization updates. Consequently the pressure levels stay constant even

when moisture leaves the column (e.g., rain). At the very end of CAM physics the change in water vapor in each column is taken into account by scaling the mixing ratio's for all tracers based on specific mixing ratios so that dry air mass and tracer mass is conserved [see Section 3.1.6 in *Neale et al.*, 2010]. This scaling does not guarantee shape-preservation. Also, the pressure in CAM physics does not take into account the mass of condensates. When using a dry-mass vertical coordinate, the coordinate surfaces (assuming dry mass is constant) remain constant throughout the physics updates and there is no need to adjust tracer mixing ratios and one can more rigorously take into account the work performed by water variables in the context of the energy cycle.

The third motivation for using a dry-mass vertical coordinate relates to total energy conservation. Currently the energy fixer in CAM is based on a dry total energy [*Williamson et al.*, 2015] that uses that same heat-capacity for dry air and water vapor, and does not include the effect of condensates. To move towards a more accurate treatment of energy in CAM, a first step is to develop a dynamical core based on equations of motion conserving an energy that properly represents water vapor as well as condensates. This is most easily done when using a dry-mass vertical coordinate so that the energies associates with all water variables are clearly separated.

In this paper we present a version of the SE dynamical core using a dry-mass vertical coordinate, includes condensate-loading, and the continuous equations of motion conserve a comprehensive moist total energy that includes all prognostic water variables and their respective heat capacities in the thermodynamic equation. As this paper serves as documentation for the CESM2 version of SE we also provide details on the spectral-element method and viscosity operators. In section 2 the continuous equations of motion are derived which involves a detailed discussion of moist thermodynamics in the presence of condensates. The axial angular momentum (AAM) and total energy conservation properties of this system of equations is also discussed. In section 3 the discretized equations of motion with focus on the vertical discretization in dry-mass vertical coordinates are documented. Details on the horizontal SE discretization on the cubed-sphere are presented. Last there is the results section 4 where the new dynamical core is validated in idealized setups. First using a moist baroclinic wave with simple warm-rain micro-physics and secondly in a CAM6 aqua-planet setup. The computational performance of CAM-SE is also discussed in section 4. The paper ends with summary and conclusions in section 5.

2 Continuous equations

Before writing the continuous equations of motion using a dry-mass vertical coordinate, we first need to discuss the representation of water variables (section 2.1), discuss the ideal gas law and derive the thermodynamic equation for a mixture containing all water variables not just water vapor (section 2.2). The discussion of the equations of motion in the presence of water vapor, cloud liquid and ice closely follows *Staniforth et al.* [2006]. Thereafter dry mass vertical coordinate is defined in section 2.4. more details on other sections

2.1 Representation of water phases in terms of dry and wet (specific) mixing ratios

Define the dry mixing ratios for the water variables (vapor 'wv', cloud liquid 'cl', cloud ice 'ci', rain 'rn' and snow 'sw')

$$m^{(\ell)} \equiv \frac{\rho^{(\ell)}}{\rho^{(d)}}, \text{ where } \ell = \text{`}wv\text{`}, \text{`}cl\text{`}, \text{`}ci\text{`}, \text{`}rn\text{`}, \text{`}sw\text{`} \tag{1}$$

where $\rho^{(d)}$ is the mass of dry air per unit volume of moist air and $\rho^{(\ell)}$ is the mass of the water substance of type ℓ per unit volume of moist air. Note that the mixing ratio for dry air is one: $m^{(d)} \equiv \frac{\rho^{(d)}}{\rho^{(d)}} = 1$. By moist air we refer to air containing dry air, water vapor,

cloud liquid, cloud ice, rain amount and snow amount. For notational purposes define the set of all components of air

$$\mathcal{L}_{all} = \{`d`, `wv`, `cl`, `ci`, `rn`, `sw`\}, \tag{2}$$

a set only referring to all water variables,

$$\mathcal{L}_{water} = \{`wv`, `cl`, `ci`, `rn`, `sw`\}, \tag{3}$$

and a set referring to all condensates (non-gas components of water)

$$\mathcal{L}_{cond} = \{`wv`, `cl`, `ci`, `rn`, `sw`\}. \tag{4}$$

The density of a unit volume of moist air is related to the dry air density through

$$\rho = \rho^{(d)} \left(\sum_{\ell \in \mathcal{L}_{all}} m^{(\ell)} \right). \tag{5}$$

Mixing ratio's can also be specified in terms of density per density of moist air, in other words, specific/moist mixing ratios

$$q^{(\ell)} \equiv \frac{\rho^{(\ell)}}{\rho}, \text{ where } \ell = `wv`, `cl`, `ci`, `rn`, `sw`. \tag{6}$$

where, in particular, $q^{(wv)}$ is the specific humidity.

It is straight forward to convert between moist and dry mixing ratios

$$m^{(\ell)} = \frac{q^{(\ell)}}{1 - \sum_{\ell \in \mathcal{L}_{water}} q^{(\ell)}}, \tag{7}$$

$$q^{(\ell)} = \frac{m^{(\ell)}}{\sum_{\ell \in \mathcal{L}_{all}} m^{(\ell)}}. \tag{8}$$

Note that if water vapor undergoes a phase change to rain and leaves the column, then the specific/wet mixing ratios change but the dry mixing ratios do not.

2.2 Ideal gas law and virtual temperature

In this section the ideal gas law is derived for moist air containing condensates. Part of that derivation is the definition of virtual temperature.

If we assume that moist air obeys Amagat's law (or the law of partial volumes) then a unit volume of moist air $V = 1$ is the sum the volume of dry air and the volumes of the different forms of water in the air

$$V = \sum_{\ell \in \mathcal{L}_{all}} V^{(\ell)}. \tag{9}$$

Now let $\alpha \equiv \frac{1}{\rho}$ denote the specific volume of moist air, let $\hat{\alpha}^{(gas)}$ be the specific volume of the gaseous components of moist air (the volume of water vapor and dry air per unit mass of water vapor and dry air), let $\hat{\alpha}^{(cl)}$ be the specific volume of cloud liquid (i.e. volume occupied by unit mass of cloud liquid), and similarly for cloud ice, rain and snow. Then we can write (9) in terms of densities and specific volumes

$$\rho\alpha = \rho^{(gas)}\hat{\alpha}^{(gas)} + \sum_{\ell \in \mathcal{L}_{cond}} \rho^{(\ell)}\hat{\alpha}^{(\ell)}, \tag{10}$$

where $\rho^{(gas)} = \rho^{(d)} + \rho^{(wv)}$. Note that $\hat{\alpha}^{(\ell)} \neq \frac{1}{\rho^{(\ell)}}$ since $\rho^{(\ell)}$ is defined in terms mass of ℓ per unit volume of moist air and not mass of ℓ per unit volume of water phase ℓ. Dividing (10) with $\rho^{(d)}$ and substituting (1) yields

$$\left(\sum_{\ell} m^{(\ell)} \right) \alpha = \left(1 + m^{(wv)} \right) \hat{\alpha}^{(gas)} + \sum_{\ell \in \mathcal{L}_{cond}} m^{(\ell)}\hat{\alpha}^{(\ell)}. \tag{11}$$

The ideal gas law for the gaseous components, using Dalton's law of partial pressures, is

$$p = p^{(d)} + p^{(wv)} = \rho^{(d)} R^{(d)} T + \rho^{(wv)} R^{(wv)} T, \tag{12}$$

where $p^{(d)}$ is the dry pressure and $p^{(wv)}$ is the water vapor pressure. We may write (12) in terms of $\rho^{(gas)}$ by multiplying (12) with $\frac{\rho^{(gas)}}{\rho^{(gas)}}$ and write the equation in terms of mixing ratios

$$p = \rho R^{(d)} T \rho^{(gas)} \left(\frac{\rho^{(d)}}{\rho^{(gas)}} + \frac{\rho^{(wv)}}{\rho^{(gas)}} \frac{R^{(wv)}}{R^{(d)}} \right) = \frac{R^{(d)} \rho^{(gas)} T \left(1 + \frac{1}{\epsilon} m^{(wv)}\right)}{\left(1 + m^{(wv)}\right)}. \tag{13}$$

where $\epsilon \equiv \frac{R^{(d)}}{R^{(wv)}}$. Since (12) holds for the gaseous components only we may substitute $\frac{1}{\rho^{(gas)}}$ with $\hat{\alpha}^{(gas)}$ to get:

$$p = \frac{R^{(d)} T \left(1 + \frac{1}{\epsilon} m^{(wv)}\right)}{\left(1 + m^{(wv)}\right) \hat{\alpha}^{(gas)}}. \tag{14}$$

Using (11) to eliminate $\left(1 + m^{(wv)}\right) \hat{\alpha}^{(gas)}$ in (14) and simplifying yields

$$p = \rho R^{(d)} T_v, \tag{15}$$

where the virtual temperature is given by

$$T_v = T \left[\frac{1 + \frac{1}{\epsilon} m^{(wv)}}{1 + m^{(wv)} + \sum_{\ell \in \mathcal{L}_{cond}} m^{(\ell)} \left(1 - \frac{\hat{\alpha}^{(\ell)}}{\alpha}\right)} \right]. \tag{16}$$

The ratio of the density of moist air to the density of the condensates are negligible (e.g., the terms $\frac{\hat{\alpha}^{(cl)}}{\alpha}$ and $\frac{\hat{\alpha}^{(ci)}}{\alpha}$ are of order 10^{-3} or less) hence the formula for virtual temperature is simplified to

$$T_v = T \left(\frac{1 + \frac{1}{\epsilon} m^{(wv)}}{\sum_{\ell \in \mathcal{L}_{all}} m^{(\ell)}} \right). \tag{17}$$

2.3 Thermodynamic equation

The first law of thermodynamics for a mixture of dry air, water vapor, cloud liquid water, cloud ice, rain and snow is given by

$$\frac{\sum_{\ell \in \mathcal{L}_{all}} c_v^{(\ell)} m^{(\ell)}}{\sum_{\ell \in \mathcal{L}_{all}} m^{(\ell)}} \delta T + p \delta \alpha = \delta Q, \tag{18}$$

where δQ is the amount of heat per unit mass that is supplied reversibly to the moist air, δT and $\delta \alpha$ are the moist airs temperature and specific volume changes and $c_v^{(\ell)}$ is the heat capacity at constant volume for component ℓ of moist air. Note that

$$\begin{aligned}
\left(\sum_{\ell \in \mathcal{L}_{all}} m^{(\ell)} \right) p \delta \alpha &= p \delta \left[\left(\sum_{\ell \in \mathcal{L}_{all}} m^{(\ell)} \right) \alpha \right], & (19) \\
&= (1 + m^{(wv)}) p \delta \hat{\alpha}^{(gas)}, & (20) \\
&= \left(R^{(d)} + m^{(wv)} R^{(wv)} \right) \left(\delta T - \frac{T}{p} \delta p \right). & (21)
\end{aligned}$$

where, in (19), we have assumed that $m^{(\ell)}$ is constant. To get (20) we substituted (11) into the right-hand side of (19) and assumed that cloud ice and liquid are incompressible ($\delta \hat{\alpha}^{(cl)} = 0$ and $\delta \hat{\alpha}^{(ci)} = 0$). Finally (14) has been used to substitute for $\hat{\alpha}^{(gas)}$ in (21). Using (21) in the First law of thermodynamics (18), substituting $R^{(d)} = c_v^{(d)} - c_v^{(d)}$ and $R^{(wv)} = c_p^{(wv)} - c_v^{(wv)}$, using that $c_p^{(\ell)} = c_v^{(\ell)}$ for the condensates (they are incompressible) and rearranging terms yields

$$\delta T - \frac{\left(R^{(d)} + m^{(wv)} R^{(wv)} \right)}{\left(\sum c_p^{(\ell)} m^{(\ell)} \right)} \frac{T}{p} \delta p = \frac{\left(\sum_{\ell \in \mathcal{L}_{all}} m^{(\ell)} \right)}{\left(\sum_{\ell \in \mathcal{L}_{all}} c_p^{(\ell)} m^{(\ell)} \right)} \frac{\delta Q}{T}. \tag{22}$$

Equation (22) can be written in a more familiar form

$$\delta T - \frac{R}{c_p}\frac{T}{p}\delta p = \frac{1}{c_p T}\delta Q, \tag{23}$$

if we define c_p and R as

$$c_p = \frac{\sum_{\ell\in\mathcal{L}_{all}} c_p^{(\ell)} m^{(\ell)}}{\sum_{\ell\in\mathcal{L}_{all}} m^{(\ell)}}, \tag{24}$$

$$R = \frac{\sum_{\ell\in\mathcal{L}_{all}} R^{(\ell)} m^{(\ell)}}{\sum_{\ell\in\mathcal{L}_{all}} m^{(\ell)}}. \tag{25}$$

where $R^{(\ell)} = 0$ for $\ell \in \mathcal{L}_{cond}$. Note that with these definitions of c_p and R the ideal gas law can be written as

$$p = \rho R T, \tag{26}$$

and

$$c_p = R + c_v. \tag{27}$$

The thermodynamic equation (23) may also be written in terms of full density

$$\delta T - \frac{1}{\rho\, c_p}\delta p = \frac{1}{c_p T}\delta Q. \tag{28}$$

2.4 Vertical coordinate

2.4.1 Definition

Let $\mathcal{P}_s^{(d)}$ be the surface pressure of a dry atmosphere and $\mathcal{P}_t^{(d)}$ the pressure at the model top. We assume that there is no moisture or condensate above the model top so $p_t^{(d)} = p_t^{(wv)} = \mathcal{P}_t^{(d)}$. Consider a general, terrain-following, vertical coordinate $\eta^{(d)}$ that is a function of dry atmosphere pressure $\mathcal{P}^{(d)}$

$$\eta^{(d)} = h(\mathcal{P}^{(d)}, \mathcal{P}_s^{(d)}), \tag{29}$$

where $h(\mathcal{P}s^{(d)}, \mathcal{P}s^{(d)}) = 1$ and $h(\mathcal{P}t^{(d)}, \mathcal{P}s^{(d)}) = 0$. Note that by removing the superscript (d) from the equations above so that the dry variable represent moist pressure variables then the vertical coordinate is the usual hybrid-pressure coordinate widely used in hydrostatic global modeling [*Simmons and Burridge*, 1981]. The top and bottom boundary conditions are that $\dot{\eta}\left(\mathcal{P}s^{(d)}, \mathcal{P}s^{(d)}\right) = 0$ and $\dot{\eta}\left(\mathcal{P}t^{(d)}, \mathcal{P}s^{(d)}\right) = 0$. Note that using a dry-mass vertical coordinate simplifies the coupling to physics since the dry mass coordinates do not change location if there are water-vapor (or other phase changes) in the column.

2.4.2 Dry pressure and dry atmosphere pressure

The observant reader will have noticed that we denote the dry atmosphere pressure $\mathcal{P}^{(d)}$ and not $p^{(d)}$. The moist pressure at given height z' can be computed from the hydrostatic balance

$$p = \int_{z'=z}^{z'=\infty} \rho\, g\, dz', \tag{30}$$

$$= \int_{z'=z}^{z'=\infty} \rho_d \left(\sum_{\ell\in\mathcal{L}_{all}} m_\ell\right) g\, dz', \tag{31}$$

$$= \sum_{\ell\in\mathcal{L}_{all}} \mathcal{P}^{(\ell)}, \tag{32}$$

where the right-hand side of (32) is the weight of dry air, water vapor, cloud liquid, cloud ice, rain and snow per unit area, respectively:

$$\mathcal{P}^{(\ell)} = \int_{z'=z}^{z'=\infty} \rho_d\, m_\ell\, g\, dz'. \tag{33}$$

Using Dalton's law of partial pressures, (32) can be written as

$$p^{(d)} + p^{(wv)} = \sum_{\ell \in \mathcal{L}_{all}} \mathcal{P}^{(\ell)}. \tag{34}$$

From (34) it is clear that in the presence of condensate one can not equate $p^{(d)}$ with $\mathcal{P}^{(d)}$ and equate $p^{(wv)}$ with $\mathcal{P}^{(wv)}$. The dry pressure and water vapor pressure are both affected by the weight of the condensates even though the condensates do not exert a pressure. Hence the dry pressure $p^{(d)}$ is different from the pressure in a dry atmosphere $\mathcal{P}^{(d)}$. The hydrostatic balance of a dry atmosphere, written in terms of differentials, is given by

$$d\mathcal{P}^{(d)} = -\rho_d g dz, \tag{35}$$

whereas, in a moist atmosphere, a dry pressure hydrostatic equation does not hold

$$dp^{(d)} \neq -\rho_d g dz. \tag{36}$$

The differential of the moist pressure can be written in terms of the dry atmosphere pressure though:

$$dp = -\rho g\, dz = -\rho_d \left(\sum_{\ell \in \mathcal{L}_{all}} m_\ell \right) g\, dz = d\mathcal{P}^{(d)} \left(\sum_{\ell \in \mathcal{L}_{all}} m_\ell \right). \tag{37}$$

2.5 Equations of motion

The $\eta^{(d)}$-coordinate adiabatic and frictionless atmospheric primitive equations assuming floating Lagrangian vertical coordinates [*Starr*, 1945; *Lin*, 2004] can be written as

$$\frac{\partial \vec{v}}{\partial t} + (\zeta + f)\, \hat{\vec{k}} \times \vec{v} + \nabla_{\eta^{(d)}} \left(\frac{1}{2} \vec{v}^2 + \Phi \right) + \frac{1}{\rho} \nabla_{\eta^{(d)}} p = 0, \tag{38}$$

$$\frac{\partial T}{\partial t} + \vec{v} \cdot \nabla_{\eta^{(d)}} T - \frac{1}{c_p \rho} \omega = 0, \tag{39}$$

$$\frac{\partial}{\partial t} \left(\frac{\partial \mathcal{P}^{(d)}}{\partial \eta^{(d)}} m^{(\ell)} \right) + \nabla_{\eta^{(d)}} \cdot \left(\frac{\partial \mathcal{P}^{(d)}}{\partial \eta^{(d)}} m^{(\ell)} \vec{v} \right) = 0, \quad \ell = \text{`}d\text{`}, \text{`}wv\text{`}, \text{`}cl\text{`}, \text{`}ci\text{`}, \tag{40}$$

where ρ is the full density $\sum_{\ell \in \mathcal{L}_{all}} \rho^{(\ell)}$, p is moist pressure, Φ is the geopotential height ($\Phi = g\, z$, where g is the gravitational constant), $\hat{\vec{k}}$ is the unit vector normal to the surface of the sphere, $\zeta = \hat{\vec{k}} \cdot \nabla \times \vec{v}$ is vorticity, f Coriolis parameter, and $\omega = Dp/Dt$ is the pressure vertical velocity.

The prognostic equations for $\vec{v}$, the temperature T, pseudo density of a dry atmosphere $\frac{\partial \mathcal{P}^{(d)}}{\partial \eta^{(d)}}$, and pseudo tracer density $\frac{\partial \mathcal{P}^{(d)}}{\partial \eta^{(d)}} m^{(\ell)}$ are solved with the diagnostic equation for geopotential height (hydrostatic balance)

$$\frac{\partial \Phi}{\partial \eta^{(d)}} = -\frac{R^{(d)}\, T_v}{p} \frac{\partial p}{\partial \eta^{(d)}}, \tag{41}$$

where

$$\frac{\partial p}{\partial \eta^{(d)}} = \frac{\partial \mathcal{P}^{(d)}}{\partial \eta^{(d)}} \left(\sum_{\ell \in \mathcal{L}_{all}} m^{(\ell)} \right). \tag{42}$$

For diagnosing vertical pressure velocity ω we note that

$$\omega(\eta^{(d)}) = \frac{dp}{dt}(\eta^{(d)}), \tag{43}$$

$$= \int_{\eta^{(d)}}^{\eta^{(d)}=0} \frac{d}{dt} \left(\frac{\partial p}{\partial \eta^{(d)}} \right) d\eta^{(d)}, \tag{44}$$

$$= \int_{\eta^{(d)}}^{\eta^{(d)}=0} \frac{\partial}{\partial t} \left(\frac{\partial p}{\partial \eta^{(d)}} \right) d\eta^{(d)} + \int_{\eta^{(d)}}^{\eta^{(d)}=0} \vec{v} \cdot \nabla \left(\frac{\partial p}{\partial \eta^{(d)}} \right) d\eta^{(d)}. \tag{45}$$

2.6 Hyperviscosity and frictional heating

2.6.1 Viscosity operator [NEEDS WORK!]

The spectral-element method does not have implicit diffusion hence hyperviscosity operators are applied to the prognostic variables [Taylor reference]. On the right-hand side of the momentum equations (38) viscous terms $\nu\nabla^4\left(\nabla\times\vec{v}\right)+\nu_{div}\nabla^4\left(\nabla\cdot\vec{v}\right)$ are added. The velocity field is split into vorticity and divergence to allow for increased damping of divergent modes. The pseudo-density and temperature are damped with $\nu\nabla^4\left\{\frac{\partial p}{\partial\eta^{(d)}}\right\}$ and $\nu\nabla^4 T$. The horizontal hyperviscosity operator can be applied on η_d-surfaces, $\nu\nabla^4=\nu\nabla^4_{\eta_d}$, but it may be advantageous to apply the hyperviscosity operator on approximate pressure surfaces

$$\nu\nabla^4\Xi=\nu\nabla^4_{\eta_d}-\frac{\partial\Xi}{\partial p}\nu\nabla^4_{\eta_d}p,\qquad \Xi=\vec{v},T, \tag{46}$$

[p.58 in *Neale et al.*, 2010] to reduce spurious diffusion over steep topography.

2.6.2 Reference pressure damping

Patrick

2.6.3 Frictional heating

Let the $\delta\vec{v}$ be the change in the velocity vector due to diffusion of momentum. Then the change in kinetic energy due hyperviscosity applied to $\vec{v}$ is $\frac{1}{2}\rho\vec{v}\cdot\delta\vec{v}$. This kinetic energy is converted to a heating rate by adding a heating term $\delta\mathcal{T}$ in the thermodynamic equation corresponding to the kinetic energy change

$$\rho c_p\delta\mathcal{T}=-\frac{1}{2}\rho\vec{v}\cdot\delta\vec{v}\Rightarrow\delta\mathcal{T}=-\frac{1}{c_p}\left(\vec{v}\cdot\delta\vec{v}\right), \tag{47}$$

[p.71 in *Neale et al.*, 2010]. As shown in the results section this term is rather large and therefore important for good energy conservation characteristics of the dynamical core.

2.7 Global conservation

Below it is shown that the continuous equations of motion, that include the effect of condensates, conserve AAM and total energy. For the derivations first note that adding the continuity equations $\ell=$ 'd', 'wv', 'cl', 'ci' (40), using hydrostatic balance (41) and ideal gas law (15), yields a moist air continuity

$$\frac{\partial}{\partial t}\left[\rho\left(\frac{\partial z}{\partial\eta^{(d)}}\right)\right]+\nabla_{\eta^{(d)}}\cdot\left[\vec{v}\rho\left(\frac{\partial z}{\partial\eta^{(d)}}\right)\right]=0, \tag{48}$$

or, equivalently, in Lagrangian form

$$\frac{D}{Dt}\left[\rho\left(\frac{\partial z}{\partial\eta^{(d)}}\right)\delta A\right]=0, \tag{49}$$

where δA is a horizontal area of a Lagrangian air parcel so that $\nabla\cdot\vec{v}=\frac{1}{\delta A}\frac{D}{Dt}\left(\delta A\right)$, and $\frac{D}{Dt}=\frac{\partial}{\partial t}+\vec{v}\cdot\nabla$ is the material/total derivative.

2.7.1 Axial angular momentum (AAM)

The conservation law for angular momentum is derived in spherical coordinates for which the zonal momentum equation takes the form

$$\frac{Du}{Dt}=\frac{uv\tan\varphi}{r}+2\Omega v\sin\varphi-\frac{1}{\rho r\cos\varphi}\frac{\partial p}{\partial\lambda}, \tag{50}$$

where u and v the zonal and meridional velocity components, respectively, φ is latitude and λ longitude, Ω rotation rate of Earth ($f = 2\Omega\sin\varphi$), and r is the mean radius of Earth.

The conservation law for AAM, $\mathcal{M} = (u + \Omega r\cos\varphi)\, r\cos\varphi$, can be conveniently derived using the Lagrangian form. Consider the material derivative of $\mathcal{M}$ multiplied by the volume of a Lagrangian air parcel, $\rho\left(\frac{\partial z}{\partial \eta^{(d)}}\right)\delta A$

$$\frac{D}{Dt}\left[\rho\left(\frac{\partial z}{\partial \eta^{(d)}}\right)\delta A\,(u + \Omega r\cos\varphi)\, r\cos\varphi\right]. \tag{51}$$

Using the chain rule, continuity equation on the form (49), the equality $v = r\frac{D\varphi}{Dt}$ and substituting (50), one can obtain an evolution equation for AAM

$$\frac{D}{Dt}\left[\rho\left(\frac{\partial z}{\partial \eta^{(d)}}\right)\delta A\,\mathcal{M}\right] = -\left(\frac{\partial z}{\partial \eta^{(d)}}\right)\frac{\partial p}{\partial \lambda}, \tag{52}$$

or, equivalently, in Eulerian form

$$\frac{\partial}{\partial t}\left[\rho\left(\frac{\partial z}{\partial \eta^{(d)}}\right)\mathcal{M}\right] + \nabla_{\eta_d}\cdot\left[\vec{v}\rho\left(\frac{\partial z}{\partial \eta^{(d)}}\right)\mathcal{M}\right] = -\left(\frac{\partial z}{\partial \eta^{(d)}}\right)\frac{\partial p}{\partial \lambda}. \tag{53}$$

Repeatedly using the chain rule one can show that the right-hand side of (52) and (53) can be written as

$$-\left(\frac{\partial z}{\partial \eta^{(d)}}\right)\frac{\partial p}{\partial \lambda} = -\frac{\partial}{\partial \lambda}\left[\left(\frac{\partial z}{\partial \eta^{(d)}}\right)p\right] + p\frac{\partial}{\partial \lambda}\left(\frac{\partial z}{\partial \eta^{(d)}}\right) \tag{54}$$

$$= -\frac{\partial}{\partial \eta^{(d)}}\left(\frac{\partial z}{\partial \lambda}p\right) + \left(\frac{\partial z}{\partial \eta^{(d)}}\right)\frac{\partial p}{\partial \lambda} + p\frac{\partial}{\partial \lambda}\left(\frac{\partial z}{\partial \eta^{(d)}}\right), \tag{55}$$

$$= -\frac{\partial}{\partial \eta^{(d)}}\left(\frac{\partial z}{\partial \lambda}p\right) + \left(\frac{\partial z}{\partial \eta^{(d)}}\right)\frac{\partial p}{\partial \lambda} - \frac{\partial}{\partial \lambda}\left[p\left(\frac{\partial z}{\partial \eta^{(d)}}\right)\right] - \frac{\partial p}{\partial \lambda}\left(\frac{\partial z}{\partial \eta^{(d)}}\right). \tag{56}$$

$$= -\frac{\partial}{\partial \eta^{(d)}}\left(\frac{\partial z}{\partial \lambda}p\right) - \frac{\partial}{\partial \lambda}\left[p\left(\frac{\partial z}{\partial \eta^{(d)}}\right)\right]. \tag{57}$$

Substituting (57) on the right-hand side of (53) and integrating (53) in the horizontal and vertical we get

$$\frac{\partial}{\partial t}\int_{\eta=0}^{\eta=1}\iint_{\mathcal{D}}\left[\left(\sum_{\ell\in\mathcal{L}_{all}} m^{(\ell)}\right)\left(\frac{\partial \mathcal{P}^{(d)}}{\partial \eta^{(d)}}\right)\mathcal{M}\right]dA\, d\eta^{(d)} = -\iint_{\mathcal{D}}\left[p_s\frac{\partial z_s}{\partial \lambda}\right]dA, \tag{58}$$

where $\mathcal{D}$ is the global domain and $dA = r^2\cos\varphi d\lambda d\varphi$ is an infinitesimal spherical area. The term in the square brackets on the right-hand side of (58) is referred to as the mountain torque. In the absence of topography,$z_s = 0$m, (58) states that the angular momentum integrated over the entire domain is constant for the continuous equations of motion. Note that the AAM can be separated into a part ($\mathcal{M}_r$) associated with the relative motion of the atmosphere with respect to Earth's surface (also known as wind AAM) and another part ($\mathcal{M}_\Omega$) associated with the angular velocity Ω:

$$\mathcal{M} = \mathcal{M}_r + \mathcal{M}_\Omega = (ur\cos\varphi) + \left(\Omega r^2\cos^2\varphi\right). \tag{59}$$

2.7.2 Total energy

The derivation of the total energy equation closely follows *Kasahara* [1974] but for a dry mass vertical coordinate and inclusion of condensates in the equations of motion. The equation for the horizontal kinetic energy per unit mass, $K = \frac{1}{2}\vec{v}\cdot\vec{v}$, is derived by multiplying the momentum equations (38) with $\rho\vec{v}\left(\frac{\partial z}{\partial \eta^{(d)}}\right)$ and the continuity equation (48) with K, adding the two resulting equations and simplifying using the chain rule yields

$$\frac{\partial}{\partial t}\left[\rho\left(\frac{\partial z}{\partial \eta^{(d)}}\right)K\right] + \nabla_{\eta^{(d)}}\left[\rho\vec{v}\left(\frac{\partial z}{\partial \eta^{(d)}}\right)K\right] = -\left(\frac{\partial z}{\partial \eta^{(d)}}\right)\vec{v}\nabla_{\eta^{(d)}}p - g\rho\left(\frac{\partial z}{\partial \eta^{(d)}}\right)\vec{v}\cdot\nabla_{\eta^{(d)}}z. \tag{60}$$

For the derivation of a flux-form version of the total energy equation (that includes a geopotential term) we substitute

$$g\rho\left(\frac{\partial z}{\partial \eta^{(d)}}\right)\vec{v}\cdot\nabla_{\eta^{(d)}}z = \nabla_{\eta^{(d)}}\cdot\left[gz\vec{v}\rho\left(\frac{\partial z}{\partial \eta^{(d)}}\right)\right] - gz\nabla_{\eta^{(d)}}\cdot\left[\vec{v}\rho\left(\frac{\partial z}{\partial \eta^{(d)}}\right)\right], \tag{61}$$

$$= \nabla_{\eta^{(d)}}\cdot\left[gz\vec{v}\rho\left(\frac{\partial z}{\partial \eta^{(d)}}\right)\right] - z\nabla_{\eta^{(d)}}\cdot\left[\vec{v}\left(\frac{\partial p}{\partial \eta^{(d)}}\right)\right], \tag{62}$$

(where the hydrostatic balance equation (41) has been used on the right-hand side of (62)) on the right-hand side of (60) and rearrange terms

$$\frac{\partial}{\partial t}\left[\rho\left(\frac{\partial z}{\partial \eta^{(d)}}\right)K\right] + \nabla_{\eta^{(d)}}\cdot\left[\rho\vec{v}\left(\frac{\partial z}{\partial \eta^{(d)}}\right)(K+gz)\right] = -\left(\frac{\partial z}{\partial \eta^{(d)}}\right)\vec{v}\nabla_{\eta^{(d)}}p - z\nabla_{\eta^{(d)}}\cdot\left[\vec{v}\left(\frac{\partial p}{\partial \eta^{(d)}}\right)\right]. \tag{63}$$

Now, by multiplying the thermodynamic equation (39) with $\rho\frac{\partial z}{\partial \eta^{(d)}}c_p$ and the continuity equation (48) with c_pT, adding the resulting equations and simplifying using the chain rule yields

$$\frac{\partial}{\partial t}\left[\rho\left(\frac{\partial z}{\partial \eta^{(d)}}\right)c_pT\right] + \nabla_{\eta^{(d)}}\left[\rho\vec{v}\left(\frac{\partial z}{\partial \eta^{(d)}}\right)c_pT\right] = \left(\frac{\partial z}{\partial \eta^{(d)}}\right)\omega. \tag{64}$$

By using that $\omega \equiv \frac{\partial p}{\partial t} + \vec{v}\cdot\nabla_{\eta^{(d)}}p$, using the chain rule and the continuity equation (48) , one can show that

$$\left(\frac{\partial z}{\partial \eta^{(d)}}\right)\omega = \frac{\partial}{\partial \eta^{(d)}}\left(z\frac{\partial p}{\partial t}\right) + \left(\frac{\partial z}{\partial \eta^{(d)}}\right)\vec{v}\nabla_{\eta^{(d)}}p + z\nabla_{\eta^{(d)}}\cdot\left[\vec{v}\frac{\partial p}{\partial \eta^{(d)}}\right]. \tag{65}$$

Substituting (65) on the right-hand side of (64) and adding the resulting equation to (63), the two terms on the right-hand side of (63) cancel the two last terms on the right-hand side of (65) and we get the total energy equation

$$\frac{\partial}{\partial t}\left[\rho\left(\frac{\partial z}{\partial \eta^{(d)}}\right)\left(K+c_pT\right)\right] + \nabla_{\eta^{(d)}}\left[\rho\vec{v}\left(\frac{\partial z}{\partial \eta^{(d)}}\right)\left(K+gz+c_pT\right)\right] = \frac{\partial}{\partial \eta^{(d)}}\left(z\frac{\partial p}{\partial t}\right). \tag{66}$$

This equation is in the same form as (5.7) in *Kasahara* [1974] but ρ, c_p and p include the effect of condensates. Noting that

$$c_pT\rho\left(\frac{\partial z}{\partial \eta^{(d)}}\right) = c_vT\rho\left(\frac{\partial z}{\partial \eta^{(d)}}\right) + gz\rho\left(\frac{\partial z}{\partial \eta^{(d)}}\right), \tag{67}$$

where we have used the ideal gas law on the form (26), chain rule and hydrostatic equation on the form (41), the total energy equation can be written on the form

$$\frac{\partial}{\partial t}\left[\rho\left(\frac{\partial z}{\partial \eta^{(d)}}\right)(K+c_vT+gz)\right] + \nabla_{\eta^{(d)}}\left[\rho\vec{v}\left(\frac{\partial z}{\partial \eta^{(d)}}\right)\left(K+gz+c_pT\right)\right] = -\frac{\partial}{\partial \eta^{(d)}}\left(p\frac{\partial z}{\partial t}\right). \tag{68}$$

As an aside it is noted that in a z-based vertical coordinate (for a moment assume $\eta^{(d)} \equiv z$), if integrating (68) in the vertical and using that z is constant at the model top (z_{top}) and surface (z_s) we get

$$\frac{\partial}{\partial t}\int_{z=z_s}^{z=z_{top}}(K+c_vT+gz)\,\rho dz + \nabla_z\cdot\int_{z=z_s}^{z=z_{top}}\vec{v}\left(K+gz+c_pT\right)\rho dz = 0. \tag{69}$$

Note the clear separation of kinetic (K), potential (gz) and internal (c_vT) energy. Integrating (69) in the horizontal over the entire sphere the flux term drops out, and it is clear that the total energy is conserved for the frictionless and adiabatic system of equations.

For the global integral of the total energy equation in a dry-mass vertical coordinate, we substitute the hydrostatic relation on the form (41) into (66), integrate in the vertical and use that the pressure at the model top is constant,

$$\frac{1}{g}\frac{\partial}{\partial t}\int_{\eta=0}^{\eta=1}\left(\sum_{\ell\in\mathcal{L}_{all}}m^{(\ell)}\right)\left(\frac{\partial\mathcal{P}^{(d)}}{\partial \eta^{(d)}}\right)\left(K+c_pT\right)d\eta^{(d)}$$

$$+\frac{1}{g}\nabla_{\eta^{(d)}}\cdot\int_{\eta=0}^{\eta=1}\vec{v}\left(\sum_{\ell\in\mathcal{L}_{all}}m^{(\ell)}\right)\left(\frac{\partial\mathcal{P}^{(d)}}{\partial \eta^{(d)}}\right)\left(K+gz+c_pT\right)d\eta^{(d)} = -z_s\frac{\partial p_s}{\partial t}, \tag{70}$$

which can also be written as

$$\frac{1}{g}\frac{\partial}{\partial t}\int_{\eta=0}^{\eta=1}\left(\frac{\partial \mathcal{P}^{(d)}}{\partial \eta^{(d)}}\right)\sum_{\ell\in\mathcal{L}_{all}}\left[m^{(\ell)}\left(K+c_p^{(\ell)}T+\Phi_s\right)\right]d\eta^{(d)} + \frac{1}{g}\nabla_{\eta^{(d)}}\cdot\int_{\eta=0}^{\eta=1}\vec{v}\left(\frac{\partial \mathcal{P}^{(d)}}{\partial \eta^{(d)}}\right)\sum_{\ell\in\mathcal{L}_{all}}\left[m^{(\ell)}\left(K+c_p^{(\ell)}T+gz\right)\right]d\eta^{(d)}=0. \quad (71)$$

by expanding c_p using (24), re-arranging terms and using that $\Phi_s = gz_s$ is time-independent and that

$$p_s = \int_{\eta=0}^{\eta=1}\sum_{\ell\in\mathcal{L}_{all}}\left(\frac{\partial \mathcal{P}^{(d)}}{\partial \eta^{(d)}}\right)m^{(\ell)}d\eta^{(\eta)}. \quad (72)$$

Note that the energy terms (inside square brackets) in (71) separate into dry air, water vapor, cloud liquid and cloud ice components

$$\left(\frac{\partial \mathcal{P}^{(d)}}{\partial \eta^{(d)}}\right)\sum_{\ell\in\mathcal{L}_{all}}\left[m^{(\ell)}\left(K+c_p^{(\ell)}T+\Phi_s\right)\right]. \quad (73)$$

Similarly for the flux term in the second square brackets on the left-hand side of (71). Integrating (71) over the entire sphere results in

$$\frac{1}{g}\frac{\partial}{\partial t}\int_{\eta=0}^{\eta=1}\iint_{\mathcal{D}}\left(\frac{\partial \mathcal{P}^{(d)}}{\partial \eta^{(d)}}\right)\sum_{\ell\in\mathcal{L}_{all}}\left[m^{(\ell)}\left(K+c_p^{(\ell)}T+\Phi_s\right)\right]dAd\eta^{(d)}=0. \quad (74)$$

We note that the CAM physics package energy fixer assumes that the 'perfect' adiabatic dynamical core conserves an energy where $c_p^{(wv)} = c_p^{(d)}$, $c_p^{(\ell)} = 0$ for $\ell =$ 'cl', 'ci' and $m^{(\ell)} = 0$ for $\ell =$ 'cl', 'ci' [*Williamson et al.*, 2015]. In other words, the CAM energy fixer uses a dry total energy. The discrepancy between the more comprehensive energy formula (74) and the CAM physics formula for total energy is about 0.5 W/m^2 [*Taylor*, 2011].

3 Discretized equations of motion

3.1 Vertical discretization

In the vertical the atmosphere is discretized into $nlev$ floating Lagrangian layers. The vertical index is 1 for the upper most level and $nlev$ in the lower most level. The level interfaces are referred to as half-levels so that layer k is bounded by interface level $k + 1/2$ and $k - 1/2$. Since we are using a dry-mass vertical reference coordinate, the dry atmosphere reference pressure at the layer interfaces is defined in terms of the hybrid coefficients A and B that are only a function of level index

$$\mathcal{P}_{k+1/2}^{(d)} = A_{k+1/2}p_t + B_{k+1/2}\mathcal{P}_s^{(d)}, \quad (75)$$

and similarly for full levels k. Note that if the 'd' is removed from the above equation so that the levels are based on moist pressure then the vertical coordinate becomes the usual hybrid vertical coordinate used in many global hydrostatic models. Every $rsplit$ time-steps the floating Lagrangian levels the prognostic variables are remapped to the dry-mass reference coordinate (75) (see Section 3.1.5).

CAM-SE is based on a Lorenz vertical staggering so the full level prognostic variables are $\vec{v}_k$ (velocity vector), T_k (temperature), $\Delta\mathcal{P}_k^{(d)} = \mathcal{P}_{k+1/2}^{(d)} - \mathcal{P}_{k-1/2}^{(d)}$ (dry atmosphere pressure level thickness), and $\Delta\mathcal{P}_k^{(d)}m_k^{(\ell)}$ (tracer mass per unit area). At the level interfaces the geopotential, pressure, vertical velocity and density are defined. In the equations of motion the full level pressure, geopotential height, vertical velocity and density are needed and choices must be made on how these variables are derived (in discretized space) from the prognostic variables. Here we use the energy and angular momentum conserving method of *Simmons and Burridge* [1981] to compute these quantities at full levels as discussed in the sections below. For simplicity we do not discretize in the horizontal yet.

3.1.1 Pressure

The half-level moist pressure is

$$p_{k+1/2} = p_t + \sum_{j=1}^{nlev} \Delta\mathcal{P}_j^{(d)} \left(\sum_{\ell \in \mathcal{L}_{all}} m_j^{(\ell)} \right), \tag{76}$$

where p_t is the pressure at the model top, $\eta^{(d)} = 0$. The full level moist pressure is obtained by averaging [*Simmons and Burridge*, 1981]

$$p_k = \frac{p_{k+1/2} + p_{k-1/2}}{2}. \tag{77}$$

3.1.2 Geopotential height

Discretizing (41) in the vertical yields

$$\Phi_{k+1/2} = \Phi_s + R^{(d)} \sum_j \left(\frac{T_k}{p_k} \right) \Delta p_j, \tag{78}$$

where the full pressure p_k is given in (77). The half level geopotential is computed by averaging

$$\Phi_k = \frac{\Phi_{k+1/2} + \Phi_{k-1/2}}{2}. \tag{79}$$

3.1.3 Vertical pressure velocity

The vertical pressure velocity ω is obtained by discretizing (45). The first term on the right-hand side of (45) can be computed by using the continuity equations for dry pressure level thickness and water vapor mass in each layer (40)

$$\frac{\partial}{\partial t} \left[\sum_{j=1}^{k} \Delta\mathcal{P}_j^{(d)} \left(\sum_{\ell \in \mathcal{L}_{all}} m_j^{(\ell)} \right) \right] = - \sum_{j=1}^{k} \nabla_{\eta^{(d)}} \cdot \left[\Delta\mathcal{P}_j^{(d)} \left(\sum_{\ell \in \mathcal{L}_{all}} m_j^{(\ell)} \right) \right], \tag{80}$$

so that the vertical pressure velocity at half-levels is given by

$$\omega_{k+1/2} = - \sum_{j=1}^{k} \nabla_{\eta^{(d)}} \cdot \left[\Delta\mathcal{P}_j^{(d)} \left(\sum_{\ell \in \mathcal{L}_{all}} m_j^{(\ell)} \right) \right] + \sum_{j=1}^{k} \vec{v}_k \cdot \nabla_{\eta^{(d)}} \left[\Delta\mathcal{P}_j^{(d)} \left(\sum_{\ell \in \mathcal{L}_{all}} m_j^{(\ell)} \right) \right], \tag{81}$$

and full level ω is

$$\omega_k = \frac{\omega_{k+1/2} + \omega_{k-1/2}}{2}. \tag{82}$$

3.1.4 Density

Full level density is computed from the ideal gas law (15)

$$\rho_k = \frac{p_k}{R^{(d)} T_k^{(v)}}, \tag{83}$$

where the full pressure p_k is computed as described in section 3.1.1. The virtual temperature is based on prognostic variables defined at the layer centers so simple substitution into (17) yields $T_k^{(v)}$. Similarly for the computation of $\left(c_p\right)_k$.

3.1.5 Vertical remapping

To avoid excessive deformation or even crossing of the floating Lagrangian levels, the prognostic variables defined at

$$\mathcal{P}_{k+1/2}^{(d)} = p_t + \sum_{j=1}^{k} \Delta\mathcal{P}_j^{(d)}, \tag{84}$$

are remapped back to the (Eulerian) reference levels given in (75) every $rsplit$ time-steps [*Lin*, 2004]. In the remapping process we enforce conservation of mass by mapping $m_k^{(\ell)}\Delta\mathcal{P}_k^{(d)}$ using the piecewise-parabolic method [PPM; *Colella and Woodward*, 1984] and applying a standard shape-preserving limiter to avoid unphysical (in particular negative) mixing ratios in the remapping process. The internal energy is also conserved during the remapping process by mapping $\sum_{\ell\in\mathcal{L}_{all}} c_p^{(\ell)} m_k^{(\ell)} T_k \Delta\mathcal{P}_k^{(d)}$. Note that temperature must be recovered from the internal energy using the remapped tracer values for $m_k^{(\ell)}$. A shape-preserving filter is also used for the remapping of internal energy so that an isothermal profile remains isothermal if the limiter is active on one of the water variables, $m_k^{(\ell)}$. Note that if the limiter is active at the same points for more than one of the water species then we can not guarantee preservation of an isothermal atmosphere when non-linear limiting filters are turned on [see, e.g., Section 2.5 in *Lauritzen and Thuburn*, 2012].

The moist mass-weighted velocity components, $\sum_{\ell\in\mathcal{L}_{all}} m_k^{(\ell)}\Delta\mathcal{P}_k^{(d)}u_k$ and $\sum_{\ell\in\mathcal{L}_{all}} m_k^{(\ell)}\Delta\mathcal{P}_k^{(d)}v_k$ respectively, are remapped separately. Mapping the moist mass weighted velocity components conservatively leads to an angular momentum conserving vertical remapping algorithm. For the velocity components we do not enforce shape-preservation in the vertical remapping process to reduce the amount of kinetic energy dissipation.

3.2 Horizontal discretization

The CAM-SE uses cubed-sphere geometry originally introduced by *Sadourny* [1972] to represent the planet earth. The spherical surface $\mathcal{S}$ is a patched domain, which is partitioned into non-overlapping quadrilateral elements Ω_e such that $\mathcal{S} = \cup\,\Omega_e$ (see Fig. 1). On $\mathcal{S}$ each 2D element $\Omega_e(x^1, x^2)$ defined in terms of central (gnomonic) projection angles $x^1, x^2 \in [-\pi/4, \pi/4]$, which serve as the independent variables in the computational domain. The mapping from cube to sphere results in a non-orthogonal curvilinear coordinate system on $\mathcal{S}$, with the metric tensor G_{ij} and analytic Jacobian $\sqrt{G} = |G_{ij}|^{1/2}$, $i, j \in \{1, 2\}$. A physical vector quantity such as the wind vector $\mathbf{v} = (u, v)$, defined on $\mathcal{S}$ in orthogonal lat-long coordinates, can be uniquely expressed in tensor form using conventional notations as the covariant (u_1, u_2) and contravariant (u^1, u^2) vectors using the 2×2 transformation matrix $\mathbf{D}$ associated with the gnomonic mapping such that $\mathbf{D}^T\mathbf{D} = G_{ij}$ (see *Nair et al.* [2005] for the details):

$$\begin{bmatrix} u \\ v \end{bmatrix} = \mathbf{D} \begin{bmatrix} u^1 \\ u^2 \end{bmatrix} = \mathbf{D}^{-T} \begin{bmatrix} u_1 \\ u_2 \end{bmatrix}. \tag{85}$$

The governing equations defined in familiar vector form can also be expressed in general tensor form. In order to describe the SE discretization process in simple terms, we consider the the following conservation law on $\mathcal{S}$ for an arbitrary scalar ϕ:

$$\frac{\partial\phi}{\partial t} + \nabla\cdot\mathbf{F}(\phi) = S(\phi) \quad \Rightarrow \frac{\partial\phi}{\partial t} + \frac{1}{\sqrt{G}}\left[\frac{\partial\sqrt{G}F^1}{\partial x^1} + \frac{\partial\sqrt{G}F^2}{\partial x^2}\right] = S(\phi), \tag{86}$$

where equation of the right side is a special case, the flux-form transport equation, with contravariant fluxes $(F^1, F^2) = (u^1\phi, u^2\phi)$, and $S(\phi)$ is an arbitrary source term.

3.3 SE spatial discretization in 2D

The SE solution process involves casting the PDE in Galerkin form, i.e., by multiplying (86) with a test (weight) function ψ and integrating over the domain $\mathcal{S}$,

$$\int_{\mathcal{S}} \psi \left[\frac{\partial\phi}{\partial t} + \nabla\cdot\mathbf{F}(\phi) - S(\phi)\right] d\mathcal{S} = 0. \tag{87}$$

A computational form of (87) is obtained by applying Green's theorem, resulting in the weak Galerkin form as follows:

$$\int_{\mathcal{S}} \psi\ \frac{\partial\phi}{\partial t}\, d\mathcal{S} = \int_{\mathcal{S}} \nabla\psi\cdot\mathbf{F}(\phi)\, d\mathcal{S} + \int_{\mathcal{S}} \psi\, S(\phi)\, d\mathcal{S}, \tag{88}$$

where the approximation to the solution ϕ and the test function belong to a polynomial space V^N. The SE method consists of partitioning the domain into non-overlapping elements and solving the global problem locally on each element, where the solution is approximated by using a set of basis (polynomial) functions of prescribed order N. A basic assumption used in SE (or continuous Galerkin) method is that the global basis corresponding to (88) is C^0 continuous. Therefore the problem (88) can be solved locally for each element Ω_e, if there is a mechanism by which the solution maintains C^0 continuity at the element boundaries as required by the SE discretization.

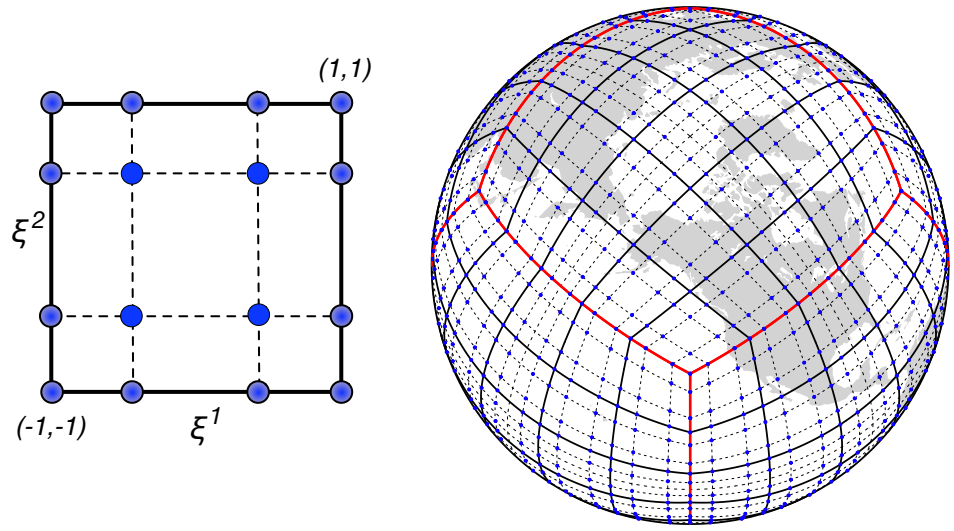

Figure 1. The left panel shows the Gauss-Lobatto-Legendre (GLL) grid with $N_p \times N_p$ quadrature points defined on a standard element $[-1,1]^2$, where $N_p = 4$. The right panel shows the cubed-sphere ($\mathcal{S}$) grid system tiled with $6N_e^2$ spectral elements Ω_e, where N_e is the number of elements in each coordinate direction on a panel. Each element Ω_e on $\mathcal{S}$ has the GLL grid structure.

For efficient evaluation of the integral equation (88), the SE method employs the Gauss-Lobatto-Legendre (GLL) quadrature rule for integrals and collocation differentiation for derivative operators. All the corresponding numerical operations are performed on a square $[-1,1]^2$ known as the standard (or reference) element. In order to facilitate local mesh refinement, the spectral elements Ω_e on $\mathcal{S}$ are defined as arbitrary spherical quadrilaterals in the CAM-SE grid system, which should be mapped onto the standard element. A direct way to address this problem is establishing a transformation $\mathcal{J}_e : \Omega_e \to [-1,1]^2$, where $\mathcal{J}_e$ may be considered as a composite mapping combining the gnomonic and the quadrilateral to standard-element mapping. Let the Jacobian associated with the composite mapping be $J_e = J_e(\sqrt{G})$. Then an arbitrary surface integral on Ω_e can be expressed in terms of local coordinates $\xi^1, \xi^2 \in [-1,1]$ and the Jacobian J_e;

$$\int_{\Omega_e} \psi(x^1,x^2)\, d\Omega_e = \int_{-1}^{1}\int_{-1}^{1} J_e(\xi^1,\xi^2)\,\psi(\xi^1,\xi^2)\, d\xi^1\, d\xi^2 \approx \sum_{k=0}^{N}\sum_{l=0}^{N} w_k w_l\, J_e(\xi_k^1,\xi_l^2)\,\psi(\xi_k^1,\xi_l^2), \tag{89}$$

where w_k, w_l are the Gauss quadrature weights.

In the case of GLL quadrature rule, the nodal points ξ_k, $k = 0,1,\ldots,N$, are the roots of the polynomial $(1-\xi^2)P'_N(\xi) = 0$, $\xi \in [-1,1]$; and the corresponding GLL

quadrature weights are given by

$$w_k = \frac{2}{N(N+1)\,[P_N(\xi_k)]^2},$$

where $P_N(\xi)$ is the Legendre polynomial of degree N. For the SE discretization it is customary to use Lagrange polynomials $h_k(\xi)$, with roots at the GLL quadrature points ξ_k, as basis functions. This setup provides discrete orthogonality for the basis function $h_k(\xi)$, which is formally defined as:

$$h_k(\xi) = \frac{(\xi^2-1)\,P'_N(\xi)}{N(N+1)\,P_N(\xi_k)\,(\xi-\xi_k)}. \tag{90}$$

Note that there are $N+1 = N_p$ GLL quadrature points in 1D, and $N_p \times N_p$ GLL points are needed for 2D spectral elements Ω_e. Figure (1) shows the GLL grid with $N_p = 4$ on the left panel, and the right panel shows the cubed-sphere grid $\mathcal{S}$ tiled with elements Ω_e, each with the GLL grid points.

A semi-discrete form of (88) on an element Ω_e can by obtained by approximating the solution as a tensor product of 1D Lagrange basis $\{h_k(\xi)\}_{k=0}^N$ such that

$$\phi|_{\Omega_e} \approx \phi^e(\xi^1,\xi^2,t) = \sum_{k=0}^{N}\sum_{l=0}^{N} \phi^e_{kl}(t)\,h_k(\xi^1)\,h_l(\xi^2), \tag{91}$$

where $\phi^e_{kl}(t) = \phi^e(\xi^1_k,\xi^2_l,t)$ are the nodal grid-point values of the solution, and defining the test function as $\psi(\xi^1,\xi^2) = h_k(\xi^1)\,h_l(\xi^2)$. By using (89) and discrete orthogonality property of $h_k(\xi)$, we get a completely decoupled system of ODEs on Ω_e, for each grid-point (k,l) we have

$$M^e_{kl}\,\frac{d}{dt}\phi^e_{kl}(t) = A^e_{kl} + S^e_{kl} \tag{92}$$

$$M^e_{kl} = \int_{-1}^{1}\int_{-1}^{1} J_e\,h_k(\xi^1)\,h_l(\xi^2)\,d\xi^1 d\xi^2 = J_e(k,l)\,w_k\,w_l \tag{93}$$

$$A^e_{kl} = \sum_{i=0}^{N} J^{(1)}_e(i,l)\,F^1_{il}\,D^{(1)}_{ik}\,w_i w_l + \sum_{i=0}^{N} J^{(2)}_e(k,i)\,F^2_{ki}\,D^{(2)}_{li}\,w_k w_i \tag{94}$$

$$S^e_{kl} = J_e(k,l)\,w_k w_l\,S(U_{kl}) \tag{95}$$

where $J^{(i)}_e = J_e\,\partial\xi^i/\partial x^i$ is the metric term and $D^{(i)}_{lk}$ is the derivative matrix $h'_k(\xi^i_l)$, along x^i-direction and $i \in \{1,2\}$. The ODEs (92) can be written a formal matrix-vector form for Ω_e as follows: *Karniadakis and Sherwin* [2013]:

$$\mathbf{M}^e\,\frac{d}{dt}\Phi^e = \mathbf{A}^e + \mathbf{S}^e + \mathbf{B}^e, \tag{96}$$

where $\mathbf{M}^e$ is the so-called mass matrix, which is a diagonal matrix with entries M^e_{kl}. $\mathbf{B}^e$ indicates the boundary terms for the element Ω_e, which is a key component linking the local and global problem (88) and enforcing C^0 continuity for solutions across element boundaries.

The global matrices associated with (88) can be obtained by summing the contributions from elemental matrices and this procedure is known as the direct stiffness summation (DSS). However the global matrices are not explicitly constructed. In practice, the DSS operation replaces interface values of two contiguous elements sharing the same physical location by the weighted sum (average) so that the boundary nodes get unique values, which maintains the continuity of the global solution across the element edges. This strategy has been adopted in CAM-SE. Note that the DSS operation does not affect interior nodal values of any element, and preserves global conservation of SE discretization for (86). The elemental discretization (96) combined with the DSS operation ($\mathcal{L}_h$) leads to the time-dependent system of ODE corresponding to (86),

$$\frac{d}{dt}\phi(t) = \mathcal{L}_h(\phi). \tag{97}$$

3.4 Mimetic discretization

[need to mention this and refer to Mark's book chapter - discuss in the context of total energy conservation too]*Taylor and Fournier* [2010]

3.5 Dissipation

In the CAM-SE model explicit fourth-order hyperviscosity ($\nu\nabla^4\phi$) used as the main stabilization mechanism. For scalar fields such as T, p, q etc., a scalar viscosity is applied, while for the horizontal momentum equations vector viscosity ($\nu\nabla^4\mathbf{v}$) is employed. The coefficient of viscosity ν may be constant or a spatially varying quantity depending on the application. High-order viscosity operator $\nu\nabla^{2m}\phi$, $m = 2, 3, \ldots$, for an arbitrary variable ϕ can be constructed by successively applying the basic Laplacian-type viscosity operator $\nabla^2(\,)$. In order to describe the SE discretization we consider the basic Laplacian without the coefficient of viscosity ν:

$$L(\phi) = \nabla^2\phi. \tag{98}$$

Integrating (98) over an element Ω_e with boundary Γ_e, using Greens method results in

$$\int_{\Omega_e} L\,\psi\; d\Omega_e = \int_{\Gamma_e} \phi\nabla\psi\; d\Gamma_e - \int_{\Omega_e} \nabla\psi\cdot\nabla\phi\; d\Omega_e \tag{99}$$

For the continuous Galekin (SE) method the boundary integral vanishes ($\psi = 0$ at the element boundaries) and the *rhs* simplifies to a surface integral. The tensor gradients in the integrand can be expressed in terms of its contravariant components $(\tilde{F}^1, \tilde{F}^2)$, using (85) such that

$$\nabla\psi\cdot\nabla\phi = \tilde{F}^1\frac{\partial\psi}{\partial x^1} + \tilde{F}^2\frac{\partial\psi}{\partial x^2}, \quad \begin{bmatrix} \tilde{F}^1 \\ \tilde{F}^2 \end{bmatrix} = \mathbf{D}^{-1}\mathbf{D}^{-T}\begin{bmatrix} \partial\phi/\partial x^1 \\ \partial\phi/\partial x^2 \end{bmatrix}. \tag{100}$$

Thus the discretization of the Laplacian for SE method can be obtained by simplifying the integral

$$\int_{\Omega_e} L\,\psi\; d\Omega_e = -\int_{\Omega_e} \nabla\psi\cdot\nabla\phi\; d\Omega_e = -\int_{\Omega_e}\left[\tilde{F}^1\frac{\partial\psi}{\partial x^1} + \tilde{F}^2\frac{\partial\psi}{\partial x^2}\right] d\Omega_e. \tag{101}$$

As in the case of (92), the weak formulation (101) can be evaluated on the standard element using the polynomial approximations (91) for ϕ, ψ on Ω_e and GLL quadrature rule. Further simplification of (101) leads to

$$L^e_{kl} = -(M^e_{kl})^{-1}\left[\sum_{i=0}^{N} J^{(1)}_e(i,l)\,\tilde{F}^1_{il}\,D^{(1)}_{ik}\,w_i w_l + \sum_{i=0}^{N} J^{(2)}_e(k,i)\,\tilde{F}^2_{ki}\,D^{(2)}_{li}\,w_k w_i\right], \tag{102}$$

where L^e_{kl} is the value of Laplacian term for a gridpoint (k,l) on Ω_e.

Note that in practice, the contravariant gradient terms in (100) are fist computed using collocation differentiation, then the weak divergence of the gradients is computed; this is followed by a DSS operation which yields the discrete Laplacian $(L(\phi^e) \Rightarrow div(grad(\phi^e)))$.

In CAM-SE the vector viscosity is handled using the vector Laplacian $\nu\nabla^2\mathbf{v}$, which is consistent with the curvilinear formulation of the momentum equation. By using the vector identity $\nabla^2\mathbf{v} = \nabla(\nabla\cdot\mathbf{v}) - \nabla\times(\nabla\times\mathbf{v})$, the coefficient of viscosity ν may be split into the viscosity corresponding to the divergence part ν_d and that for the vorticity part ν_v such that

$$\nu\nabla^2\mathbf{v} = \nu_d\,\nabla(\nabla\cdot\mathbf{v}) - \nu_v\,\nabla\times(\nabla\times\mathbf{v}). \tag{103}$$

The SE discretization of (103) is handled separately for each component using a vector test function $\vec{\psi}$ and the weak formulation:

$$\nu_d\int_{\Omega_e}\vec{\psi}\cdot\nabla(\nabla\cdot\mathbf{v})\,d\Omega_e = -\nu_d\int_{\Omega_e}(\nabla\cdot\vec{\psi})(\nabla\cdot\mathbf{v})d\Omega_e \tag{104}$$

$$-\nu_v\int_{\Omega_e}\vec{\psi}\cdot\nabla\times(\nabla\times\mathbf{v})\,d\Omega_e = -\nu_v\int_{\Omega_e}(\nabla\times\vec{\psi})\cdot(\nabla\times\mathbf{v})\,d\Omega_e, \tag{105}$$

where the line integrals along the boundaries associated with weak formulation vanishes for SE discretization. The *rhs* of the above equations are converted into equivalent tensor form for the divergence and curl terms, and discretized as in the case of (102).

3.6 Temporal discretization

In a typical CAM setup where the model top is around 40km the maximum stable time-step for solving the continuity equation for $\ell =' wv',' cl',' ci'$ (referred to as tracer advection) is limited by the maximum advective winds. The maximum stable time-step for the remaining equations of motion (thermodynamic equation, momentum equations and the continuity equation for dry air) is limited by the fastest gravity waves. Since the maximum advective winds are typically slower than the fastest gravity waves, different time-stepping methods are used for tracer advection and the remaining equations of motion. The same time-step is used but different Runge-Kutta (RK) methods are used to maintain stability.

The SE tracer advection algorithm uses a three-stage RK strong-stability-preserving (SSP) time-stepping method that ensures that the time step will preserve any shape-preserving properties preserved by the underlying spatial discretization[*Spiteri and Ruuth*, 2002]. The shape-preserving filter used is described in *Guba et al.* [2014]. The shape-preserving SE tracer advection algorithm is formally second-order accurate.[limiter applied in last RK step?]

The momentum, thermodynamic and dry air continuity equations are solved using a third-order accurate five-stage Runga-Kutta method (RK5) based on a modified version of *Kinnmark and Gray* [1984a,b] described in *Guerra and Ullrich* [2016]. The inviscid equations of motion are advanced one dynamics time-step using the RK5 method followed by the application of hyperviscosity operators by solving the advection-diffusion equation on the updated prognostic variables. Note that it is necessary to subcycle the hyperviscosity-step for stability. The viscosity terms are computed as described in section 2.6.1 and discretized using the SE method presented in 3.5.

[How is tracer advection coupled to dry air continuity equation??]

The time-steps in CAM-SE are controlled with namelist variables `se_nsplit`,`se_rsplit`, `se_hypervis_subcycle` so that the time-steps for vertical remapping Δt_{remap}, tracer advection Δt_{trac} (RK3), RK5 time-stepping for non-tracers Δt_{dyn}, and hyperviscosity Δt_{hyper} are

$$\Delta t_{remap} = \frac{\Delta t_{phys}}{\texttt{se\_nsplit}}, \tag{106}$$

$$\Delta t_{dyn} = \frac{\Delta t_{phys}}{\texttt{se\_nsplit} * \texttt{se\_rsplit}}, \tag{107}$$

$$\Delta t_{hyper} = \frac{\Delta t_{phys}}{\texttt{se\_nsplit} * \texttt{se\_rsplit} * \texttt{se\_hypervis\_subcycle}}, \tag{108}$$

$$\tag{109}$$

where Δt_{phys} is the time-step used for computing physics tendencies.

3.7 Coupling to physics

CAM-SE uses a time-split [(CHECK if it is process or time split)] in which dynamics advances the model state and then the physics tendencies are based on the dynamics updated state. The question is then how to add the physics tendencies to the dynamical core. CAM-SE supports several physics-dynamics coupling methods. Let F_X be the physics tendency for prognostic variable X in level k (for notational simplicity the vertical index is dropped). The different coupling methods are detailed below and are iden-

tified with the rather arbitrary name 'ftype'. A fuller discussion with results about different coupling methods is the content of a separate paper. Some results are given by C. Jablonowski in [*Gross et al.*, 2016, ; see section 6].

3.7.1 'ftype=0' configuration

In this case add $\Delta t_{remap} F_X$ to the state of X, advance the dynamics Δt_{remap} seconds based on the updated state, add $\Delta t_{remap} F_X$ to the dynamics updated state of X and advance the dynamics core, and so on. In other words, the forcing is split into $\frac{\Delta t_{phys}}{\Delta_{remap}}$ equal chunks and added throughout the dynamics.

The CAM parameterization package returns mixing ratio tendencies for tracers. We convert the mixing ratio tendencies to mass tendencies $F_x \Delta \mathcal{P}_k^{(d)}$ since the prognostic variable for tracers in the dynamical core is $\Delta p_k m_k^{(d)}$.

Generally modelers do not allow the tracer tendencies to drive the mixing ratio of tracers negative, however, this may happen using 'ftype=0'. If the tendency drives a mixing ratio negative the mixing ratio is set to zero. As a result not the entire tracer tendency is added leading to an inconsistency is how much mass the physics package wants to remove and the amount of tracer mass actually removed in the physics-dynamics coupling code in the dynamical core.

3.7.2 'ftype=1' configuration

In this configuration the entire physics forcing is added to the dynamics state $\Delta t_{phys} F_X$ which is equivalent to have the physics module update the model state. This coupling methods is used in CAM-FV [*Lin*, 2004]. Note that contrary to the 'ftype=0' configuration, this configuration always provides a closed mass budget for tracers in terms of physics tendencies being fully applied in the dynamical core.

3.7.3 'ftype=2' configuration

This configuration constitutes a hybrid approach where mass variables (tracers) used 'ftype=1' physics-dynamics coupling method and all other variables use the 'ftype=0' method.

4 Results

The evaluation of the SE dynamical core with CAM6 physics in AMIP configuration simulation is the subject of a separate paper. Here the new dynamical core is evaluated in simpler setups. First the new dynamical core version is compared with the old version using an idealized moist baroclinic wave without the complexity of a full physics parameterization suite. It is confirmed that the new SE dynamical core version converges to within the uncertainty of high resolution reference solutions computed with the old SE dynamical core (that has been extensively validated) and the 'workhorse' dynamical for 1° climate simulation; CAM-FV [finit-volume *Lin*, 2004]. Second, the dynamical core is evaluated in aqua-planet setup [*Neale and Hoskins*, 2000; *Williamson et al.*, 2012; *Medeiros et al.*, 2016] using CAM6 physics. .... [bla bla ...]

4.1 Idealized moist baroclinic wave with Kessler microphysics

For the validation of the new dynamical core version in a simplified setup, we use a moist variant of the dry baroclinic wave of *Ullrich et al.* [2014] with Kessler microphysics [*Kessler*, 1969]. This test case configuration was part of the Dynamical Core Model Intercomparison Project (DCMIP) 2016 test case suite [DCMIP citation]. The initialization

of the atmospheric state for the moist baroclinic wave is based on analytic expressions for T_v, $\vec{v}$, p and $q^{(wv)}$ as a function of latitude and height; (φ, z). The surface geopotential is constant, $\Phi_s = 0$, and the moist surface pressure is constant $p_s = 1000hPa$. The analytical expressions for temperature, velocity components, moist pressure and specific humidity, denoted $T_v(\varphi, z)$, $\vec{v}(\varphi, z)$, $p(\varphi, z)$, and $q^{(wv)}(\varphi, z)$, respectively, are given in Appendix A: . When using a moist vertical pressure coordinate, the full level pressures p_k of the initial condition are known from the hybrid coefficients, A_k and B_k, and one can iteratively solve for z_k given moist pressure: $p_k = p(\varphi, z_k)$ [see, *Ullrich et al.*, 2014]. Once the full level heights, $z_k(\varphi)$, are known then the specific humidity, virtual temperature and velocity components can be computed by evaluating the analytical expressions at (φ, z_k). In the DCMIP 2016 test case documentation the virtual temperature is converted to temperature using $T_v = T\left(1 + \epsilon q^{(wv)}\right)$. For a dry-mass vertical coordinate model the initialization procedure is more complicated as described below.

4.1.1 Initialization of the moist baroclinic wave using a dry-mass vertical coordinate

The challenge is to extract dry pressure from the initial state defined in terms of moist pressure and preserve a balanced initial condition. For that we write the dry atmosphere hydrostatic relation (35) in terms of specific humidity, virtual temperature and moist pressure

$$\begin{aligned}
\frac{\partial \mathcal{P}^{(d)}}{\partial z} &= -\rho_d\, g, && (110)\\
&= -\frac{\rho}{1 + m^{(wv)}}\, g, && (111)\\
&= -\frac{p}{R^{(d)} T_v} \frac{1}{\left(1 + m^{(wv)}\right)}\, g, && (112)\\
&= -\frac{p}{R^{(d)} T_v} \left(1 - q^{(wv)}\right) g, && (113)
\end{aligned}$$

where we have substituted the ideal gas law and used that $\left(\frac{1}{1+m^{(wv)}}\right) = \left(1 - q^{(wv)}\right)$ for an atmosphere not containing any condensates. Hence the dry pressure as a function of latitude, φ, and height, z, is

$$\mathcal{P}^{(d)}(\varphi, z) = p_t - \int_z^{z_t} \frac{p(\varphi, z)}{R^{(d)} T_v(\varphi, z)} \left(1 - q^{(wv)}(\varphi, z)\right) g\, dz, \tag{114}$$

where z_t is the height of the model top computed by iteratively solving (A.4) with $p(\varphi, z) = p_t$ (assuming there is no moisture above the model top). To initialize the dry pressure levels a dry surface pressure is needed. It is computed by integrating (114) with lower integral bound $z = z_s = 0\,m$ and approximating the integral using 20 point Gaussian quadrature. The dry surface pressure is shown on Figure 2. The full dry pressure levels are given in terms of the hybrid coefficients $\mathcal{P}_k^{(d)}(\varphi, z_k) = A_k p_t + B_k \mathcal{P}_s^{(d)}(\varphi, z_k)$. The height, $z_k(\varphi)$, of the full dry pressure levels are computed by iteratively solving (114) with $\mathcal{P}^{(d)}(\varphi, z) = \mathcal{P}_k^{(d)}(\varphi, z_k)$. Once the heights are known the virtual temperature and velocity components can be computed by evaluating the analytical expressions at (φ, z_k) as is done for the moist vertical coordinate initialization. If we do the same for specific humidity then the moist surface pressure (which is a diagnostic when using dry-mass vertical coordinates) deviates more than 1 Pa in the tropics from the analytical value of 1000hPa (see Figure 2). As a result a spurious zonal signal in surface pressure with the same amplitude as the initial gravity waves appears in the simulations. Hence specific humidity must be initialized more carefully in order to obtain a more balanced initial condition which is discussed in the next paragraph.

As for $\mathcal{P}^{(d)}$, the weight of water vapor $\mathcal{P}^{(d)}$ per unit area can be written as

$$\mathcal{P}^{(wv)}(\varphi, z) = -\int_z^{z_t} \frac{p(\varphi, z)}{R^{(d)} T_v(\varphi, z)} q^{(wv)}(\varphi, z)\, g\, dz, \tag{115}$$

so that the moist pressure (in the absence of condensates) at half levels can be computed as the sum of dry air and water vapor pressures

$$p(\varphi, z_{k+1/2}) = \mathcal{P}^{(d)}(\varphi, z_{k+1/2}) + \mathcal{P}^{(wv)}(\varphi, z_{k+1/2}), \tag{116}$$

where $z_{k+1/2}$ is computed by the same iterative procedure as for full levels. An integrated value for water vapor in a layer can now be computed from

$$m^{(wv)}(\varphi, z_k) = \frac{p(\varphi, z_{k+1/2}) - p(\varphi, z_{k-1/2})}{\mathcal{P}^{(d)}(\varphi, z_{k+1/2}) - \mathcal{P}^{(d)}(\varphi, z_{k-1/2})} - 1. \tag{117}$$

Using this method for initializing the mixing ratio for water vapor the moist surface pressure is within 0.01 Pa of the analytical value of 10^5 Pa (see Figure 2). Once $m^{(wv)}(\varphi, z_k)$ the temperature $T(\varphi, z_k)$ can recovered from $T_v(\varphi, z_k)$ by using (17).

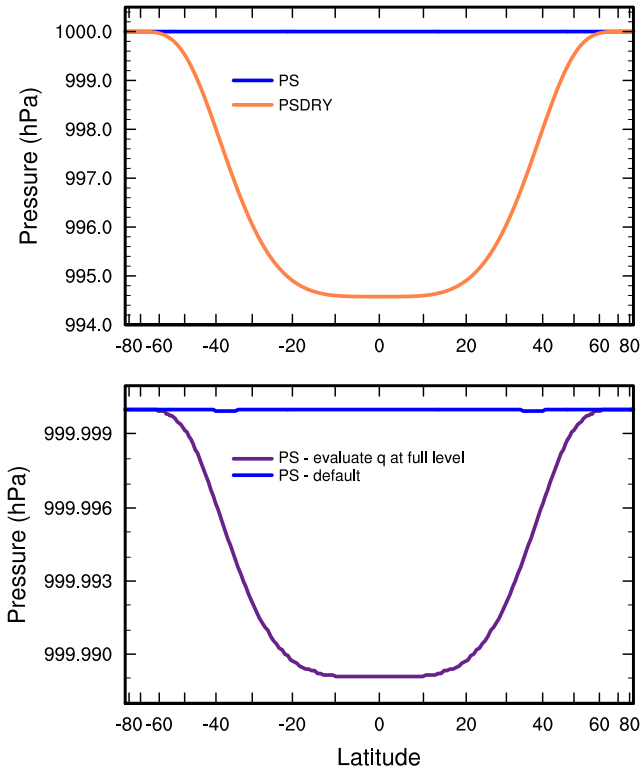

Figure 2. (Upper) Zonally averaged dry (orange) and moist (blue) surface pressure as a function of latitude for the numerically computed initial condition for the moist baroclinic wave at 1° horizontal resolution and 30 levels (CAM5 configuration). Due to increased water vapor towards the Equator the dry surface pressure decreases whereas the moist surface pressure is constant. (lower) Same as the upper plot but showing moist surface pressure where water vapor has been initialized by evaluating the analytic specific humidity formula at full levels (purple) and initializing the mixing ratio for water vapor in terms of moist and dry pressures at half levels which effectively integrates humidity over the layer (blue). Note that the upper and lower plots have different scales on the y-axis.

4.1.2 Simulation results

As part of the 'CESM simpler models' effort started by *Polvani et al.* [2017], the baroclinic wave setup has been implemented rigorously in the CESM in the sense that the

configuration easily runs from CESM without code configurations using the '**FKESSLER** compset'. For instructions on how to run the moist baroclinic wave with Kessler microphysics see *Lauritzen and Goldhaber* [2017]. Since the test case configuration has been implemented in the full CESM, the dynamical core interacts with the physics module as in full climate model simulations. Hence the global energy fixer is invoked [*Williamson et al.*, 2015] and for the dynamical cores using a moist pressure vertical coordinate there is an adjustment of specific humidity to conserve water after the moist physics updates [see Section 3.1.6 in *Neale et al.*, 2010]. The intent of this implementation is to evaluate the dynamical core in simplified setup but exactly as the dynamical core is configured for comprehensive climate simulations.

Figure 3 shows the evolution of the moist baroclinic wave at day 10 using the CAM-FV [Finite-Volume; *Lin*, 2004] dynamical core, CAM-HOMME dynamical core based on a moist vertical coordinate and the new dynamical core version (CAM-SE). The CAM-HOMME and CAM-SE (CESM2-SE) dynamical cores not only differ in terms of vertical coordinates but also in terms of hyperviscosity and the formula used for the heat-capacity in the thermodynamic equation. CAM-HOMME uses $c_p^{(d)}$ whereas CAM-SE (CESM2.0-SE) uses the comprehensive formula (24) that includes the heat capacity of water vapor.

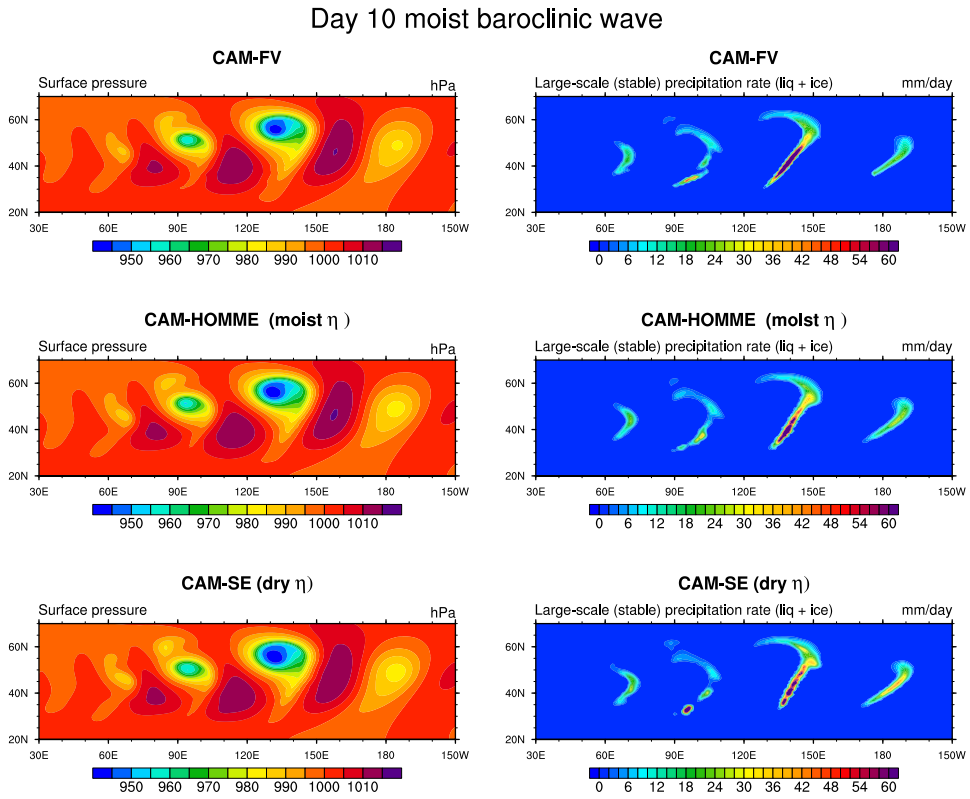

Figure 3. Left column shows moist surface pressure at day 10 for the moist baroclinic wave test case for (row 1) the finite-volume dynamical core, (row 2) CAM-HOMME version of the SE dynamical core based on a moist pressure vertical coordinate and (row 3) the dry-mass vertical coordinate version of SE presented in this paper. Rights column is the same as the left but for large-scale precipitation rate.

To provide a more quantitative measure of the difference between the moist baroclinic wave simulations, the l_2 difference norm of p_s between two simulations is computed as the time varying global integral in spherical coordinates:

$$l_2\left(p_s(t)\right) = \left[\frac{1}{4\pi}\int_0^{2\pi}\int_{-\frac{\pi}{2}}^{\frac{\pi}{2}} \left(p_{s_1}(\lambda,\varphi,t) - p_{s_0}(\lambda,\varphi,t)\right)^2 \cos(\varphi)\, d\varphi\, d\lambda\right]^{\frac{1}{2}}. \tag{118}$$

The l_2 difference norm between CAM-SE and CAM-HOMME is shown in Figure 4 for the 1° and $\frac{1}{4}^\circ$ resolution simulations. The l_2 norms for the 1° and $\frac{1}{4}^\circ$ simulations have similar time varying magnitudes. As the baroclinic waves evolves, the l_2 norms grow to a maximum on the order of 1 hPa by day 15. To assess the significance of the l_2 norms, an l_2 norm that serves as an estimate of the uncertainty of a high resolution reference simulation is computed following *Jablonowski and Williamson* [2006]. The uncertainty in the reference is taken as the l_2 between a pair of $\frac{1}{4}^\circ$ resolution moist baroclinic wave simulations using different dynamical cores, CAM-SE and CAM-FV. At a $\frac{1}{4}^\circ$ resolution, the moist baroclinic wave solutions are converged to within a tolerable level of error (not shown), and therefore comparison between dynamical cores serves as an estimate of the uncertainty in the reference solutions arising from model imperfections.

The black curve in Figure 4 is the l_2 difference norm between CAM-SE and CAM-FV at approximately a $\frac{1}{4}^\circ$ resolution. l_2 values that fall below the uncertainty in the reference are considered insignificant. The l_2 between CAM-SE and CAM-HOMME generally lie near or below the uncertainty in the reference solution, indicating the differences between CAM-SE and CAM-HOMME are insignificant for the case of the moist baroclinic wave. This is consistent with the corresponding time varying, global minimum in p_s for all the simulations, which illustrates that the differences between CAM-SE and CAM-HOMME are smaller than the differences arising from increasing the horizontal resolution.

4.2 APE bla bla bla

4.3 Performance

[John Dennis etc.]

5 Conclusions

A: Analytical initial condition functions

In this section the analytical expressions for the moist baroclinic wave are given. The moist surface pressure is constant $p_s = 1000\ hPa$, meridional wind component is zero, $v(\varphi, z) = 0\ m/s$, and the surface geopotential is zero, $\Phi_s(\varphi, z) = 0\ m^2/s^2$. The reference virtual temperature is given by

$$T_v(\varphi, z) = \left\{\mathcal{F}_1(z) - \mathcal{F}_2(z)\left[(\cos\varphi)^{\mathcal{K}} - \frac{\mathcal{K}}{\mathcal{K}+2}(\cos\varphi)^{\mathcal{K}+2}\right]\right\}^{-1}, \tag{A.1}$$

where

$$\mathcal{F}_1(z) = \frac{1}{T_0}\exp\left(\frac{\Gamma z}{T_0}\right) + \left(\frac{T_0 - T_P}{T_0 T_P}\right)\left[1 - 2\left(\frac{zg}{bR^{(d)}T_0}\right)^2\right]\exp\left[-\left(\frac{zg}{bR^{(d)}T_0}\right)^2\right] \tag{A.2}$$

$$\mathcal{F}_2(z) = \frac{(\mathcal{K}+2)}{2}\left(\frac{T_E - T_P}{T_E T_P}\right)\left[1 - 2\left(\frac{zg}{bR^{(d)}T_0}\right)^2\right]\exp\left[-\left(\frac{zg}{bR^{(d)}T_0}\right)^2\right], \tag{A.3}$$

with $T_0 = \frac{1}{2}(T_E + T_P)$. Parameter $T_E = 310\ \mathcal{K}$ is the temperature at the Equatorial surface, $T_P = 240\ \mathcal{K}$ is the polar surface temperature, $\mathcal{K} = 3$ is the jet width parameter, $b = 2$ is the jet half-width parameter, and $\Gamma = 0.005\ K/m$ is the lapse rate.

To maintain hydrostatic balance, the pressure is given by:

$$p(\varphi, z) = p_0 \exp\left[-\frac{g}{R^{(d)}}\left(\mathcal{F}_3(z) - \mathcal{F}_4(z)\mathcal{I}_T(\varphi)\right)\right] \tag{A.4}$$

where

$$\mathcal{F}_3(z) = \frac{1}{\Gamma}\left[\exp\left(\frac{\Gamma z}{T_0}\right) - 1\right] + z\left(\frac{T_0 - T_P}{T_0 T_P}\right)\exp\left[-\left(\frac{zg}{bR^{(d)}T_0}\right)^2\right] \tag{A.5}$$

$$\mathcal{F}_4(z) = \frac{(\mathcal{K}+2)}{2}\left(\frac{T_E - T_P}{T_E T_P}\right) z \exp\left[-\left(\frac{zg}{bR^{(d)}T_0}\right)^2\right]. \tag{A.6}$$

To define the zonal velocity component define the great circle distance between (λ, φ) and (λ_p, φ_p):

$$r(\lambda, \varphi; \lambda_p, \varphi_p) = a \arccos\left(\sin\varphi \sin\varphi_p + \cos\varphi \cos\varphi_p \cos(\lambda - \lambda_p)\right). \tag{A.7}$$

The zonal velocity component is

$$u(\varphi, z) = -\Omega a \cos(\varphi) + \sqrt{(\Omega a \cos(\varphi))^2 + a\cos(\varphi)U(\varphi, z)} + u'(\lambda, \varphi, z), \tag{A.8}$$

where the zonally symmetric part of the velocity field is given by

$$U(\varphi, z) = \frac{g\mathcal{K}}{a}\mathcal{F}_4(z)\left[(\cos\varphi)^{\mathcal{K}-1} - (\cos\varphi)^{\mathcal{K}+1}\right] T_v(\varphi, z), \tag{A.9}$$

$a = 6371.22\ m$ is the mean radius of Earth and angular velocity is $\Omega = \frac{2\pi}{86164}\ \frac{1}{s}$ (denominator is length of day is seconds), and $u'(\lambda, \varphi, z)$ is the exponential bell-shaped perturbation to the zonally balanced velocity field

$$u'(\lambda, \varphi, z) = \begin{cases} U_p Z(z) \exp\left[-\left(\frac{r(\lambda,\varphi;\lambda_p,\varphi_p)}{r_p}\right)^2\right], & \text{if } r(\lambda, \varphi; \lambda_p, \varphi_p) < r_p, \\ 0, & \text{otherwise,} \end{cases} \tag{A.10}$$

where perturbation velocity is $U_p = 1\ m/s$, longitude/latitude of the zonal wind perturbation centerpoint is (λ_p, φ_p)=$(\pi/9, 2\pi/9)$=(20°E,40°N), and

$$Z(z) = \begin{cases} 1 - 3\left(\frac{z}{z_p}\right)^2 + 2\left(\frac{z}{z_p}\right)^3, & \text{if } z \le z_p, \\ 0, & \text{otherwise,} \end{cases} \tag{A.11}$$

where $z_p = 15000\ m$ is the maximum height of the zonal wind perturbation. The specific humidity (moist mixing ratio for water vapor) is specified in terms of moist pressure (as the vertical variable)

$$q^{(wv)}(\lambda, \varphi, p) \quad = \quad \begin{cases} q_0 \exp\left[-\left(\frac{\varphi}{\varphi_w}\right)^4\right] \exp\left[-\left(\frac{p-p_0}{p_w}\right)^2\right], & \text{if } p > p_0/10, \\ q_t, & \text{otherwise.} \end{cases} \tag{A.12}$$

where $p_w = 340\ hPa$ is a pressure width parameter, $q_0 = 0.018\ kg/kg$ is maximum specific humidity, $q_t = 1.0 \times 10^{-12}\ kg/kg$ is specific humidity above artificial tropopause, $\varphi_w = 2\pi/9$ is the specific humidity latitudinal width parameter. In addition to water vapor the Kessler microphysics water species are cloud liquid, $m^{(cl)}$, and rain water, $m^{(rw)}$. Both are initialized to zero kg/kg.

Acknowledgments

= enter acknowledgments here =

References

Bacmeister, J. T., P. H. Lauritzen, A. Dai, and J. E. Truesdale (2012), Assessing possible dynamical effects of condensate in high resolution climate simulations, *Geophys. Res. Lett.*, *39*(L04806).

Bacmeister, J. T., M. F. Wehner, R. B. Neale, A. Gettelman, C. Hannay, P. H. Lauritzen, J. M. Caron, and J. E. Truesdale (2013), Exploratory high-resolution climate simulations using the community atmosphere model (cam), *J. Climate*, *27*(9), 3073–3099, doi: 10.1175/JCLI-D-13-00387.1.

Baer, F., H. Wang, J. J. Tribbia, and A. Fournier (2006), Climate modeling with spectral elements, *Mon. Wea. Rev.*, *134*(12), 3610–3624, doi:10.1175/MWR3360.1.

Colella, P., and P. R. Woodward (1984), The piecewise parabolic method (PPM) for gas-dynamical simulations, *J. Comput. Phys.*, *54*, 174–201.

Erath, C., P. H. Lauritzen, J. H. Garcia, and H. M. Tufo (2012), Integrating a scalable and efficient semi-Lagrangian multi-tracer transport scheme in HOMME, *Procedia Computer Science*, *9*, 994–1003.

Evans, K., P. H. Lauritzen, S. Mishra, R. Neale, M. A. Taylor, and J. J. Tribbia (2012), AMIP simulations wiht the CAM4 spectral element dynamical core, *J. Climate*, in press.

Fournier, A., M. A. Taylor, and J. J. Tribbia (2004), The spectral element atmosphere model (SEAM): High-resolution parallel computation and localized resolution of regional dynamics, *Mon. Wea. Rev.*, *132*(3), 726–748.

Gross, M., H. Wan, P. J. Rasch, P. M. Caldwell, D. L. Williamson, D. Klocke, C. Jablonowski, D. R. Thatcher, N. Wood, M. Cullen, B. Beare, M. Willett, F. Lemarié, E. Blayo, S. Malardel, P. Termonia, A. Gassmann, P. H. Lauritzen, H. Johansen, C. M. Zarzycki, K. Sakaguchi, and R. Leung (2016), Recent progress and review of issues related to Physics Dynamics Coupling in geophysical models, *ArXiv e-prints*.

Guba, O., M. Taylor, and A. St-Cyr (2014), Optimization-based limiters for the spectral element method, *J. Comput. Phys.*, *267*(0), 176 – 195, doi:http://dx.doi.org/10.1016/j.jcp.2014.02.029.

Guerra, J. E., and P. A. Ullrich (2016), A high-order staggered finite-element vertical discretization for non-hydrostatic atmospheric models, *Geosci. Model Dev.*, *9*(5), 2007–2029, doi:10.5194/gmd-9-2007-2016.

Hurrell, J. W., M. M. Holland, P. R. Gent, S. Ghan, J. E. Kay, P. J. Kushner, J.-F. Lamarque, W. G. Large, D. Lawrence, K. Lindsay, W. H. Lipscomb, M. C. Long, N. Mahowald, D. R. Marsh, R. B. Neale, P. Rasch, S. Vavrus, M. Vertenstein, D. Bader, W. D. Collins, J. J. Hack, J. Kiehl, and S. Marshall (2013), The community earth system model: A framework for collaborative research, *Bulletin of the American Meteorological Society*, *94*(9), 1339–1360, doi:10.1175/BAMS-D-12-00121.1.

Jablonowski, C., and D. L. Williamson (2006), A baroclinic instability test case for atmospheric model dynamical cores, *Q. J. R. Meteorol. Soc.*, *132*, 2943–2975.

Karniadakis, G., and S. Sherwin (2013), *Spectral/hp element methods for computational fluid dynamics*, 2 ed., 1–686 pp., Oxford University Press.

Kasahara, A. (1974), Various vertical coordinate systems used for numerical weather prediction, *Mon. Wea. Rev.*, *102*(7), 509–522.

Kessler, E. (1969), On the distribution and continuity of water substance in atmospheric circulations, *Meteorol. Monogr.*, *10*(32), 88.

Kinnmark, I. P., and W. G. Gray (1984a), One step integration methods of third-fourth order accuracy with large hyperbolic stability limits, *Mathematics and Computers in Simulation*, *26*(3), 181 – 188, doi:http://dx.doi.org/10.1016/0378-4754(84)90056-9.

Kinnmark, I. P., and W. G. Gray (1984b), One step integration methods with maximum stability regions, *Mathematics and Computers in Simulation*, *26*(2), 87 – 92, doi:http://dx.doi.org/10.1016/0378-4754(84)90039-9.

Lauritzen, P., and J. Thuburn (2012), Evaluating advection/transport schemes using interrelated tracers, scatter plots and numerical mixing diagnostics, *Quart. J. Roy. Met. Soc.*, *138*(665), 906–918, doi:10.1002/qj.986.

Lauritzen, P. H., and S. Goldhaber (2017), *CESM simpler models: Moist baroclinic wave with Kessler microphysics*, `http://www.cesm.ucar.edu/models/simpler-models-indev/fkessler/index.html`.

Lauritzen, P. H., M. A. Taylor, J. Overfelt, P. A. Ullrich, R. D. Nair, S. Goldhaber, and R. Kelly (2017), Cam-se-cslam: Consistent coupling of a conservative semi-lagrangian finite-volume method with spectral element dynamics, *Mon. Wea. Rev.*, *145*(3), 833–855, doi:10.1175/MWR-D-16-0258.1.

Lin, S.-J. (2004), A 'vertically Lagrangian' finite-volume dynamical core for global models, *Mon. Wea. Rev.*, *132*, 2293–2307.

Medeiros, B., D. L. Williamson, and J. G. Olson (2016), Reference aquaplanet climate in the community atmosphere model, version 5, *J. Adv. Model. Earth Syst.*, *8*(1), 406–424, doi:10.1002/2015MS000593.

Nair, R., H.-W. Choi, and H. Tufo (2009), Computational aspects of a scalable high-order discontinuous galerkin atmospheric dynamical core, *Computers & Fluids*, *38*(2), 309 – 319, doi:http://dx.doi.org/10.1016/j.compfluid.2008.04.006.

Nair, R. D., S. J. Thomas, and R. D. Loft (2005), A discontinuous galerkin global shallow water model, *Mon. Wea. Rev.*, *133*(4), 876–888, doi:10.1175/MWR2903.1.

Neale, R. B., and B. J. Hoskins (2000), A standard test for agcms including their physical parametrizations: I: the proposal, *Atmos. Sci. Lett*, *1*(2), 101–107, doi:10.1006/asle.2000.0022.

Neale, R. B., C.-C. Chen, A. Gettelman, P. H. Lauritzen, S. Park, D. L. Williamson, A. J. Conley, R. Garcia, D. Kinnison, J.-F. Lamarque, D. Marsh, M. Mills, A. K. Smith, S. Tilmes, F. Vitt, P. Cameron-Smith, W. D. Collins, M. J. Iacono, R. C. Easter, S. J. Ghan, X. Liu, P. J. Rasch, and M. A. Taylor (2010), Description of the NCAR Community Atmosphere Model (CAM 5.0), *NCAR Technical Note*, National Center of Atmospheric Research.

Polvani, L., A. Clement, B. Medeiros, J. Benedict, and I. Simpson (2017), Opening the door to simpler climate models in the commnity earth system model project, *EOS*, submitted.

Reed, K. A., J. T. Bacmeister, N. A. Rosenbloom, M. F. Wehner, S. C. Bates, P. H. Lauritzen, J. E. Truesdale, and C. Hannay (2015), Impact of the dynamical core on the direct simulation of tropical cyclones in a high-resolution global model, *Geophys. Res. Lett.*, *42*(9), 3603–3608, doi:10.1002/2015GL063974.

Sadourny, R. (1972), Conservative finite-difference approximations of the primitive equations on quasi-uniform spherical grids, *Mon. Wea. Rev.*, *100*, 136–144.

Simmons, A. J., and D. M. Burridge (1981), An energy and angular-momentum conserving vertical finite-difference scheme and hybrid vertical coordinates, *Mon. Wea. Rev.*, *109*(4), 758–766.

Spiteri, R., and S. Ruuth (2002), A new class of optimal high-order strong-stability-preserving time discretization methods, *SIAM Journal on Numerical Analysis*, *40*(2), 469–491, doi:10.1137/S0036142901389025.

Staniforth, A., A. White, N. Wood, J. Thuburn, M. Zerroukat, E. Cordero, T. Davies, and . M. Diamantakis (2006), Joy of u.m. 6.3 - model formulation, *UK Met Office Technical Note*, *15*.

Starr, V. P. (1945), A quasi-Lagrangian system of hydrodynamical equations., *J. Atmos. Sci.*, *2*, 227–237.

Taylor, M., J. Edwards, and A. St-Cyr (2008), Petascale atmospheric models for the community climate system model: new developments and evaluation of scalable dynamical cores, *J. Phys.: Conf. Ser.*, *125*, doi:10.1088/1742-6596/125/1/012023.

Taylor, M. A. (2011), Conservation of mass and energy for the moist atmospheric primitive equations on unstructured grids, in: P.H. Lauritzen, R.D. Nair, C. Jablonowski, M. Taylor (Eds.), Numerical techniques for global atmospheric models, *Lecture Notes in Computational Science and Engineering, Springer, 2010, in press.*, *80*, 357–380, doi:10.1007/978-3-642-11640-7_12.

Taylor, M. A., and A. Fournier (2010), A compatible and conservative spectral element method on unstructured grids, *J. Comput. Phys.*, *229*(17), 5879 – 5895, doi:10.1016/j.jcp.2010.04.008.

Thomas, S., and R. Loft (2000), Parallel semi-implicit spectral element methods for atmospheric general circulation models, *J. Sci. Comput.*, *15*, 499–518.

Ullrich, P. A., T. Melvin, C. Jablonowski, and A. Staniforth (2014), A proposed baroclinic wave test case for deep and shallow-atmosphere dynamical cores, *Quart. J. Royal Meteor. Soc.*, *140*(682), 1590–1602.

Williamson, D.L., M. Blackburn, B. Hoskins, K. Nakajima, W. Ohfuchi, Y. Takahashi, Y.-Y. Hayashi, H. Nakamura, M. Ishiwatari, J. McGregor, H. Borth, V. Wirth, H. Frank, P. Bechtold, N. Wedi, H. Tomita, M. Satoh, M. Zhao, I. Held, M. Suarez, M.-I. Lee, M. Watanabe, M. Kimoto, Y. Liu, Z. Wang, A. Molod, K. Rajendran, A. Kitoh, , and R. Stratton (2012), The ape atlas, *NCAR Technical Note*, *NCAR/TN-484+STR*, doi: DOI:10.5065/D6FF3QBR.

Williamson, D. L., J. G. Olson, C. Hannay, T. Toniazzo, M. Taylor, and V. Yudin (2015), Energy considerations in the community atmosphere model (cam), *J. Adv. Model. Earth Syst.*, *7*(3), 1178–1188, doi:10.1002/2015MS000448.

Zarzycki, C. M., C. Jablonowski, and M. A. Taylor (2013), Using variable-resolution meshes to model tropical cyclones in the community atmosphere model, *Mon. Wea. Rev.*, *142*(3), 1221–1239.

Zarzycki, C. M., M. N. Levy, C. Jablonowski, J. R. Overfelt, M. A. Taylor, and P. A. Ullrich (2014), Aquaplanet experiments using cam's variable-resolution dynamical core, *J. Climate*, *27*(14), 5481–5503, doi:10.1175/JCLI-D-14-00004.1.

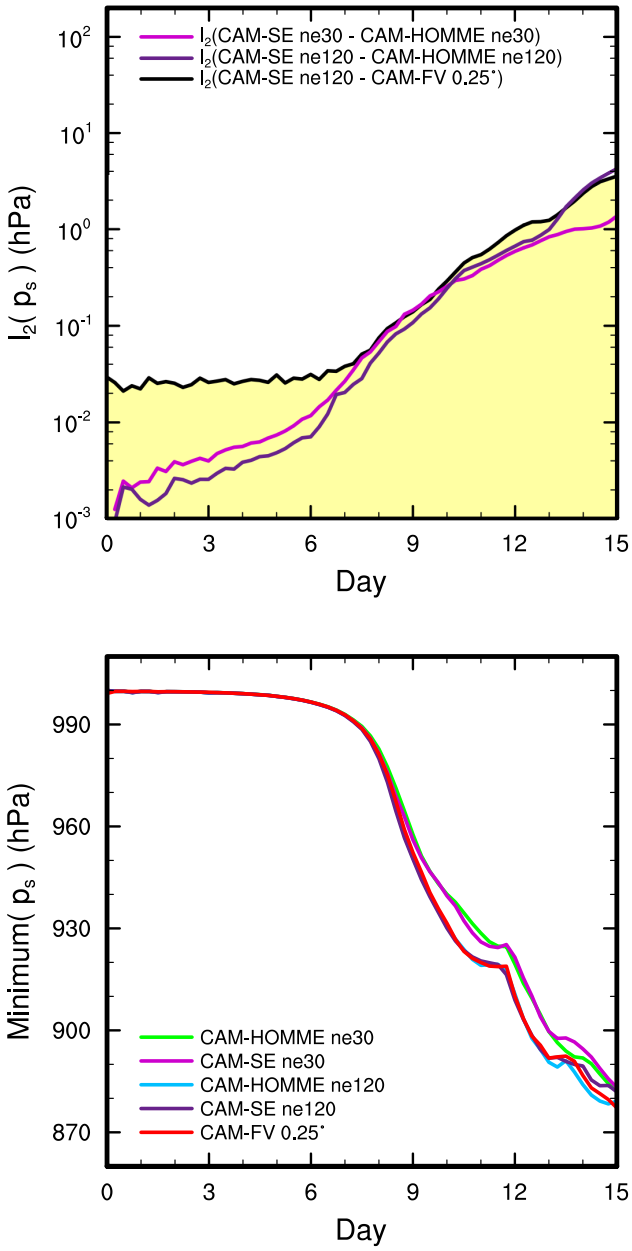

Figure 4. (Upper) l_2 difference norms of p_s in the moist baroclinic wave simulations. l_2 values lying within the yellow region fall below the estimate of the uncertainty in the reference solution (black curve). (lower) Global minimum p_s in the moist baroclinic wave simulations.